BBA - Molecular Basis of Disease 1865 (2019) 161–180

Contents lists available at ScienceDirect

BBA - Molecular Basis of Disease

journal homepage: www.elsevier.com/locate/bbadis

OAB-14, a bexarotene derivative, improves Alzheimer's disease-related pathologies and cognitive impairments by increasing β-amyloid clearance in APP/PS1 mice

Chunling Yuan[a,c,1], Xiaoli Guo[a,1], Qifan Zhou[b,1], Fangyu Du[b], Wei Jiang[d], Xiaoyu Zhou[a], Peng Liu[a], Tianyan Chi[a], Xuefei Ji[a], Jinheng Gao[b], Chengwen Chen[b], Hongli Lang[a], Jia Xu[a], Danyang Liu[a], Yang Yang[a], Shimeng Qiu[a], Xing Tang[d], Guoliang Chen[b,*], Libo Zou[a,*]

[a] Department of Pharmacology, Life Science and Biopharmaceutics School, Shenyang Pharmaceutical University, 103 Wenhua Road, Shenyang, Liaoning 110016, PR China

[b] Key Laboratory of Structure-Based Drugs Design & Discovery of Ministry of Education, School of Pharmaceutical Engineering, Shenyang Pharmaceutical University, 103 Wenhua Road, Shenyang, Liaoning 110016, PR China

[c] Department of Medicinal Chemistry, Pharmacy School, Jinzhou Medical University, Jinzhou 121001, PR China

[d] School of Pharmacy, Shenyang Pharmaceutical University, 103 Wenhua Road, Shenyang, Liaoning 110016, PR China

ARTICLE INFO

Keywords:
OAB-14
Bexarotene
Alzheimer
A beta
Hyperphosphorylated tau
BDNF

ABSTRACT

The pathogenesis of Alzheimer's disease (AD) is complex, though the clinical failures of anti-AD candidates targeting Aβ production (such as β- and γ-secretase inhibitors) make people suspect the Aβ hypothesis, in which the neurotoxicity of Aβ is undoubtedly involved. According to studies, > 95% of AD patients with sporadic AD are primarily associated with abnormal Aβ clearance. Therefore, drugs that increase Aβ clearance are becoming new prospects for the treatment of AD. Here, the novel small molecule OAB-14, designed using bexarotene as the lead compound, significantly alleviated cognitive impairments in amyloid precursor protein (APP)/presenilin 1 (PS1) transgenic mice after administration for 15 days or 3 months. OAB-14 rapidly cleared 71% of Aβ by promoting microglia phagocytosis and increasing IDE and NEP expression. This compound also attenuated the downstream pathological events of Aβ accumulation, such as synaptic degeneration, neuronal loss, tau hyperphosphorylation and neuroinflammation in APP/PS1 mice. Moreover, OAB-14 had no significant effect on body weight or liver toxicity after acute and chronic treatment. OAB-14 was well tolerated and its maximum-tolerated dose in mice was > 4.0 g/kg. Based on these findings, OAB-14 represents a promising new candidate for AD treatment.

1. Introduction

Alzheimer's disease (AD), a degenerative disease of the central nervous system, was discovered by Alois Alzheimer in 1906. According to the World Alzheimer Report 2016 [1], 46.8 million individuals had AD in 2015, and that number will reach 131.5 million by 2050. Thus, AD will cause a substantial financial burden to society and families. Current drugs used to treat AD in the clinic include donepezil, galantamine, rivastigmine and memantine; however, these drugs are not highly effective. Therefore, the development of effective interventions as treatments for AD is urgently needed.

AD is characterized by intracellular neurofibrillary tangles (NFTs), extracellular amyloid plaque deposits and neuronal loss, as well as behavioural deficits, such as learning and memory impairments. Based on mounting evidence, the accumulation of β-amyloid (Aβ) is the earliest and the most important event in AD pathogenesis [2,3], and the Aβ burden is significantly increased as the disease progresses [4]. Aβ accumulates in response to the imbalance between Aβ production and clearance. APP is degraded through the following two pathways: the non-amyloidogenic pathway and the amyloidogenic pathway. In the non-amyloidogenic pathway, α-secretase first cleaves APP, generating N-terminal sAPPα and CTF. Currently, the non-amyloidogenic pathway offers a new therapeutic option for AD because of the neuroprotective effect of sAPPα [5]. In the amyloidogenic pathway, Aβ peptides are generated from APP through a two-step proteolysis mediated by β-secretase and γ-secretase [6].

* Corresponding authors.
E-mail addresses: chenguoliang@syphu.edu.cn (G. Chen), libozou@syphu.edu.cn (L. Zou).
[1] These authors contributed equally to this work.

https://doi.org/10.1016/j.bbadis.2018.10.028
Received 27 April 2018; Received in revised form 25 October 2018; Accepted 26 October 2018
Available online 30 October 2018
0925-4439/

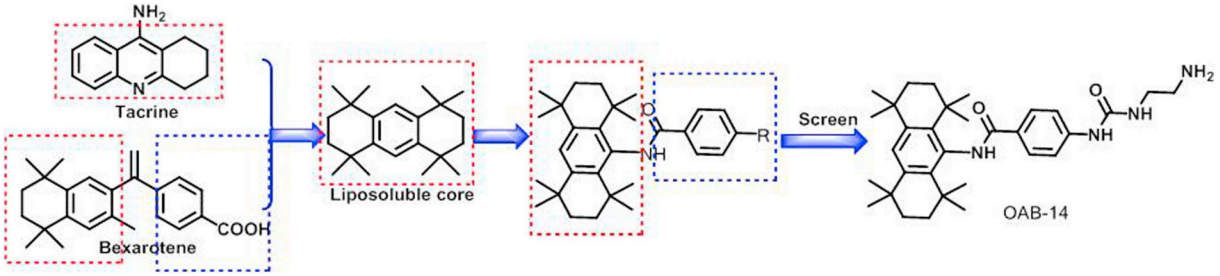

Fig. 1. Design of OAB-14 through the combination principle.

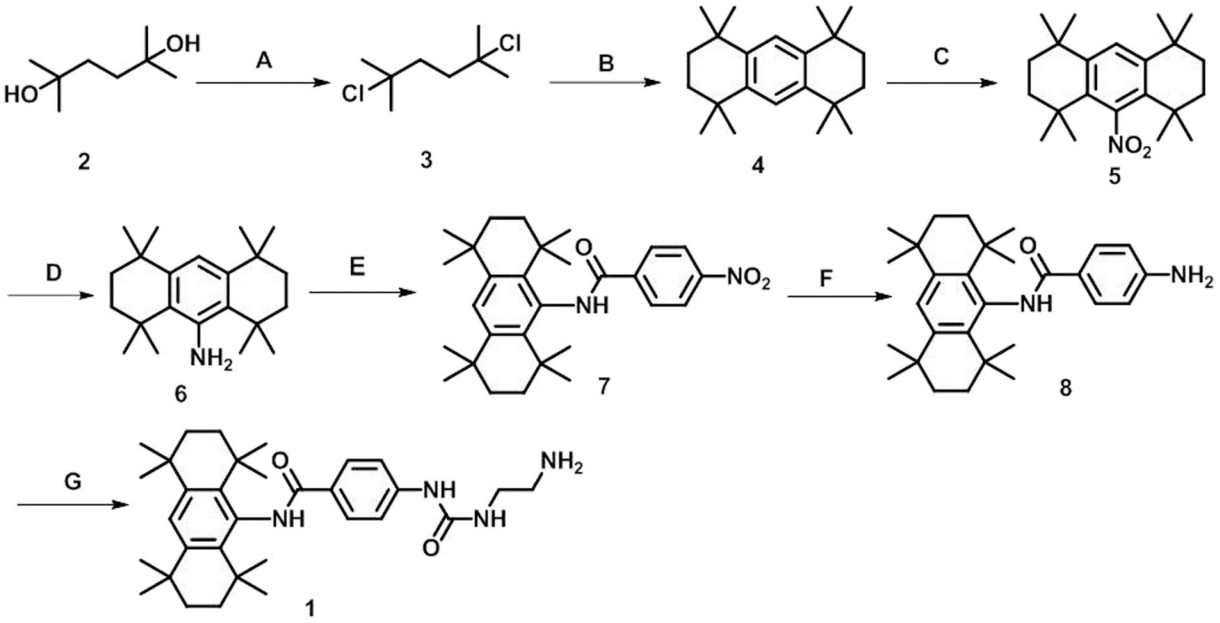

Fig. 2. Synthetic route of OAB-14. Reagents and conditions: (A) Conc. HCl, 80 °C, 1 h; (B) $AlCl_3$, DCM, r.t., 2 h; (C) CH_3COOH, Conc. HNO_3, Conc. H_2SO_4, DCM, 40 °C, 3 h; (D) Sn/HCl (gas), Conc. HCl, ethanol; (E) 4-nitrobenzoyl chloride, DMAP, Py, xylol, reflux, 12 h; (F) H_2/Pd-C, C_2H_5OH, THF, 30 °C, 25 h; (G) BTC/DCM, TEA, ethylenediamine.

Table 1
Treatment protocols.

Study	Mice (length of treatment)	Drug delivery	Treatment
T1	C57 mice APP/PS1 mice (15 days)	Gavage	Control (n = 11), peanut oil Model (n = 11), peanut oil Bexarotene (n = 11), 10 mg/ml in peanut oil OAB-14 5 mg/ml (n = 11), 10 mg/ml (n = 11), 20 mg/ml in peanut oil (n = 11) 0.1 ml/10 g (mouse weight)
T2	C57 mice APP/PS1 mice (90 days)	Gavage	Control (n = 11), 5 mice peanut oil, 6 mice 0.5%CMC-Na Model (n = 11), 5 mice peanut oil, 6 mice 0.5%CMC-Na Bexarotene (n = 11), 10 mg/ml in peanut oil OAB-14 10 mg/ml (n = 11), 20 mg/ml in peanut oil (n = 11) Donepezil (n = 11), 0.13 mg/ml in 0.5%CMC-Na 0.1 ml/10 g (mouse weight)

Familial AD accounts for < 5%, while sporadic AD, also referred to as late-onset AD, accounts for approximately 95% of total AD cases. The main aetiology of sporadic AD is substantial Aβ deposition in the brain due to normal Aβ production, but defective Aβ clearance. Recently, several clinical trials that reduced the production of Aβ using targeted drugs, such as β- or γ-secretase inhibitors, failed to improve cognitive impairments in patients with AD [7,8]. Due to the low permeability of the blood-brain barrier, the Aβ antibody only eliminated soluble Aβ in peripheral blood, which had little effect on AD treatment [9]. Therefore, small molecule therapeutic drugs that easily pass through the blood-brain barrier and improve Aβ clearance should be highly attractive.

In a study by the Landreth group [10], the administration of bexarotene, a retinoid X receptor (RXR) agonist used as a treatment for cutaneous T cell lymphoma, reduced Aβ levels in the brain and restored cognitive function in AD mouse models within only 7 days of treatment. Thus, bexarotene may be a promising treatment for AD. However, other studies [11–14] have failed to fully replicate the results reported by the Landreth group. Furthermore, bexarotene displays a large number of serious side effects, such as hepatomegaly, hypertriglyceridemia, weight loss, and central hypothyroidism, which likely result from hepatic failure. Our group designed and synthesized a series of compounds using bexarotene as the lead compound, and screened out the novel small molecule OAB-14. We examined the effects of acute and chronic OAB-14 treatments on cognitive functions and Aβ levels in brain tissues from 8-month-old amyloid precursor protein (APP)/

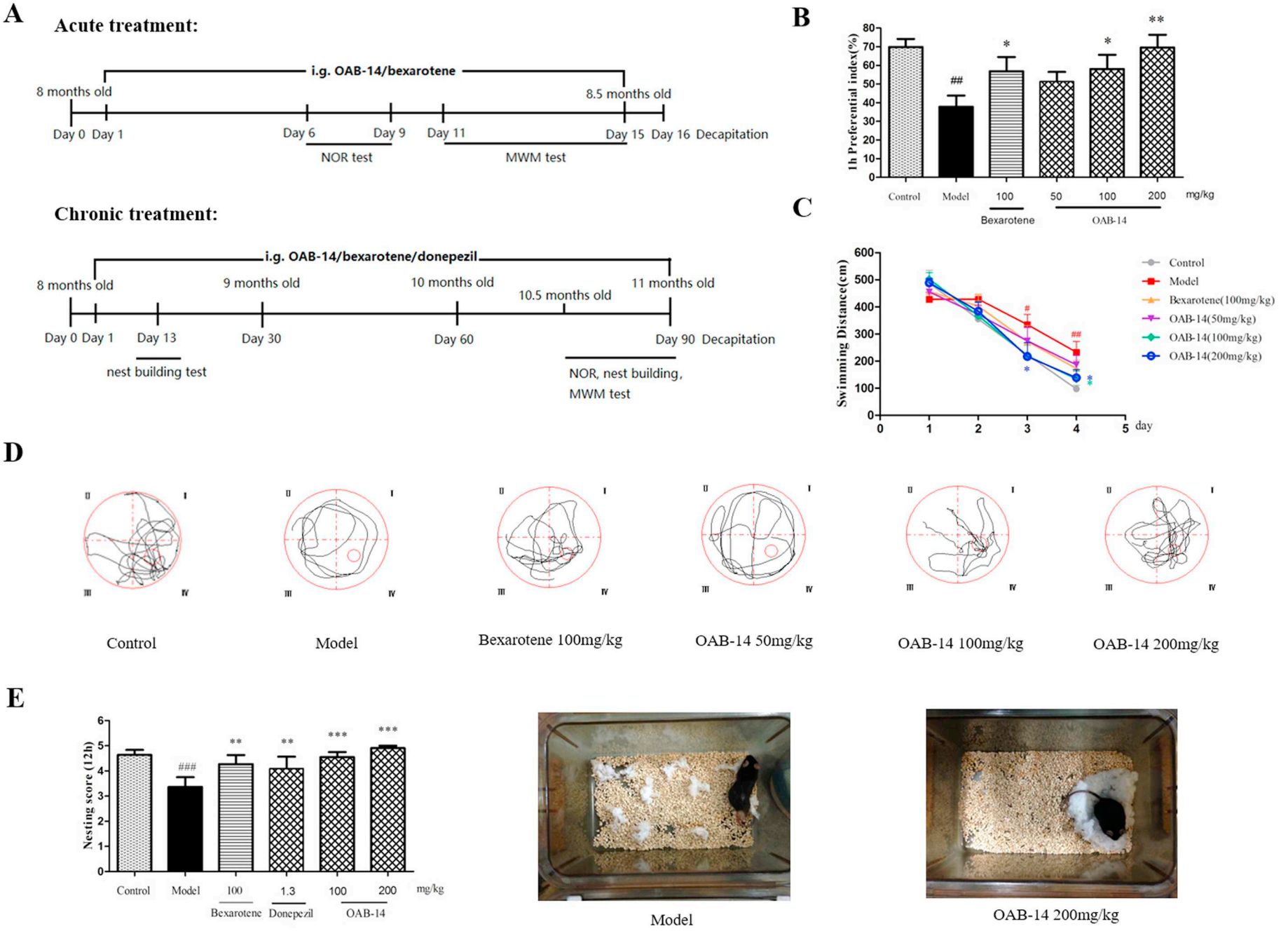

Fig. 3. OAB-14 improves cognitive impairments in APP/PS1 mice after acute treatment. (A) Experimental schedule. (B) Preferential index for 1 h in NOR test. (C) Swimming distance in the MWM test training period. (D) Swimming trace of mice in the probe test. (E) Performance in nesting test. (n = 9–10, mean ± SEM). $^{\#}p < 0.05$, $^{\#\#}p < 0.01$ or $^{\#\#\#}p < 0.001$ vs. the control group and $^{*}p < 0.05$, $^{**}p < 0.01$ or $^{***}p < 0.001$ vs. the model group.

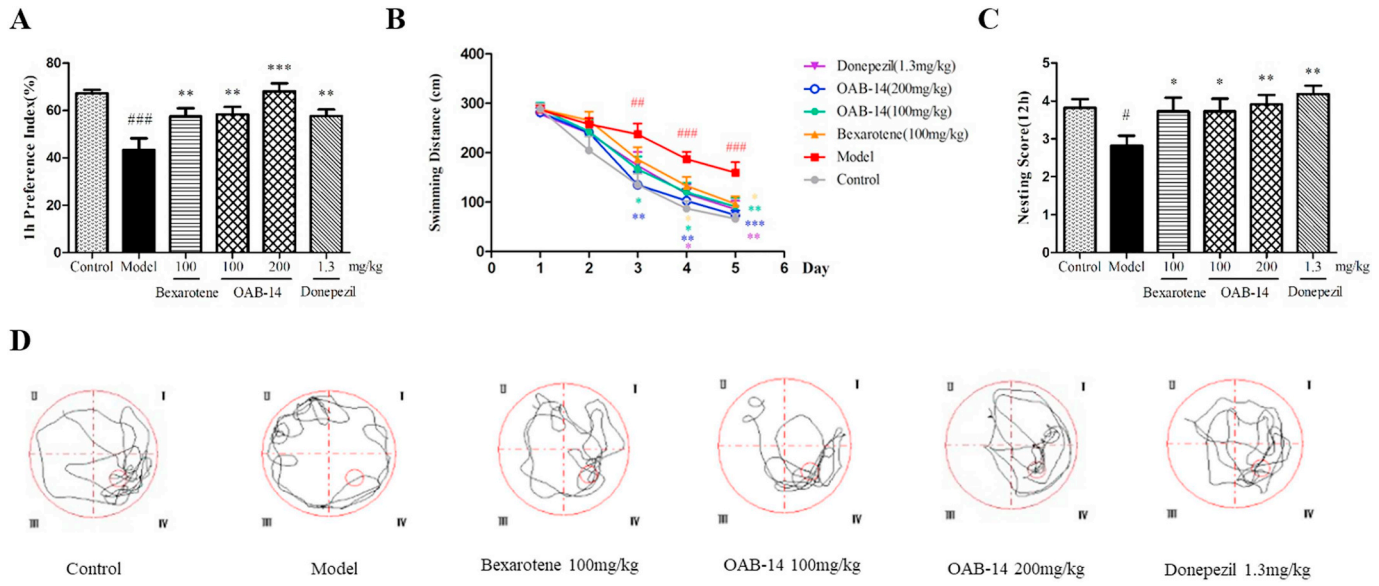

Fig. 4. OAB-14 improves cognitive impairments in APP/PS1 mice after chronic treatment. (A) Preferential index for 1 h in NOR test. (B) Swimming distance in the MWM test training period. (C) Performance in nesting test. (D) Swimming trace of mice in the probe test. (n = 9–10, mean ± SEM). $^{\#}p < 0.05$, $^{\#\#}p < 0.01$ or $^{\#\#\#}p < 0.001$ vs. the control group and $^{*}p < 0.05$, $^{**}p < 0.01$ or $^{***}p < 0.001$ vs. the model group.

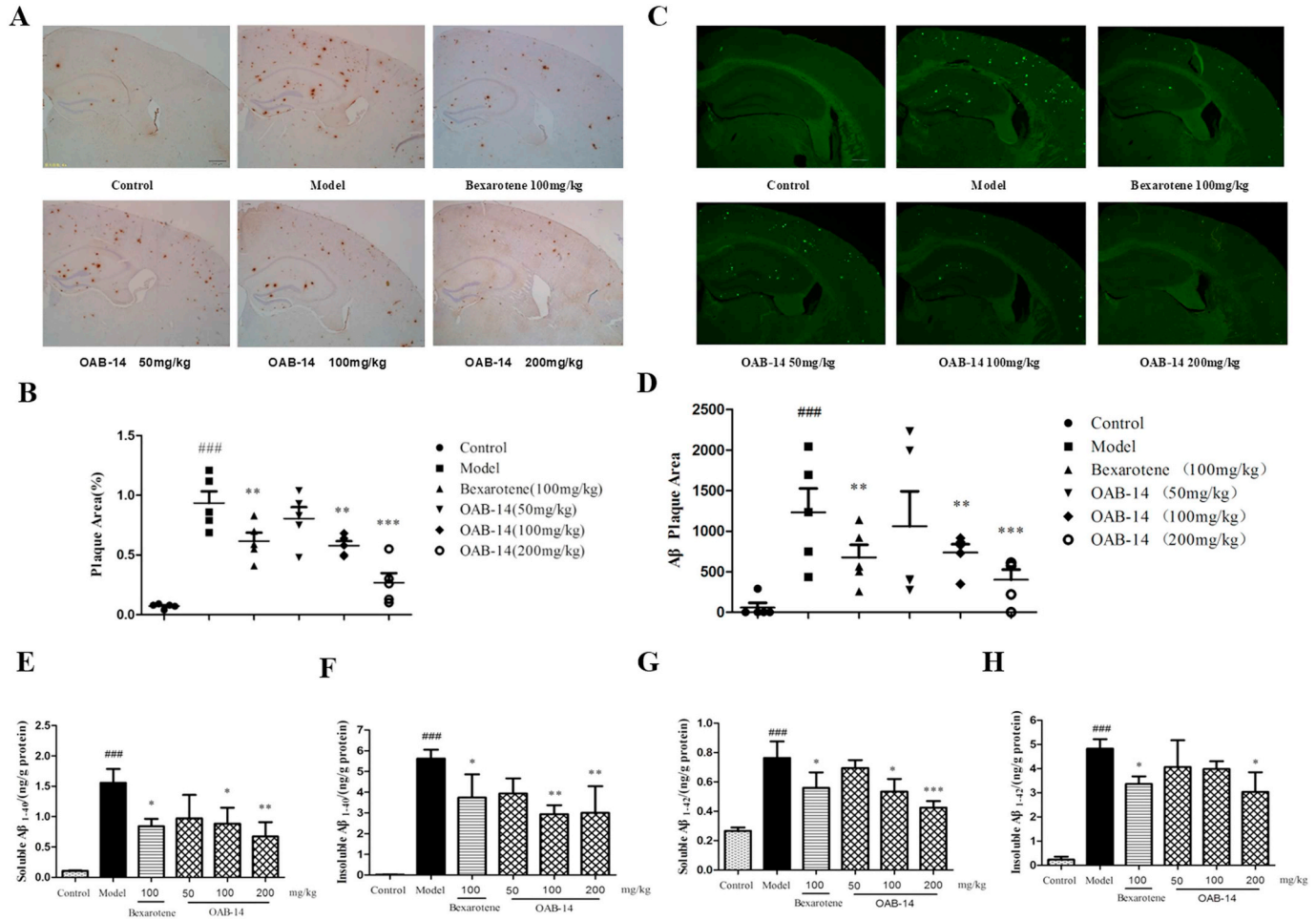

Fig. 5. OAB-14 clears Aβ in the cerebral cortex and hippocampus of APP/PS1 mice after acute treatment. (A) Aβ immunostaining (6E10) in the brain of APP/PS1 transgenic mice. Scale bars, 200 μm. (B) Quantification of the Aβ plaque (6E10) throughout the cerebral cortex and hippocampus of APP/PS1 transgenic mice. (C) Aβ thioflavin-S staining in the brain of APP/PS1 transgenic mice. Scale bars, 200 μm. (D) Quantification of the Aβ plaque area (thioflavin-S) throughout the cerebral cortex and hippocampus of APP/PS1 transgenic mice. Levels of (E) soluble $A\beta_{1–40}$, (F) insoluble $A\beta_{1–40}$, (G) soluble $A\beta_{1–42}$ and (H) insoluble $A\beta_{1–42}$ in the cortex of APP/PS1 transgenic mice detected by ELISA. Data are presented as the mean ± SEM (n = 5). $^{\#\#\#}p < 0.001$ vs. the control group and $^{*}p < 0.05$, $^{**}p < 0.01$ or $^{***}p < 0.001$ vs. the model group.

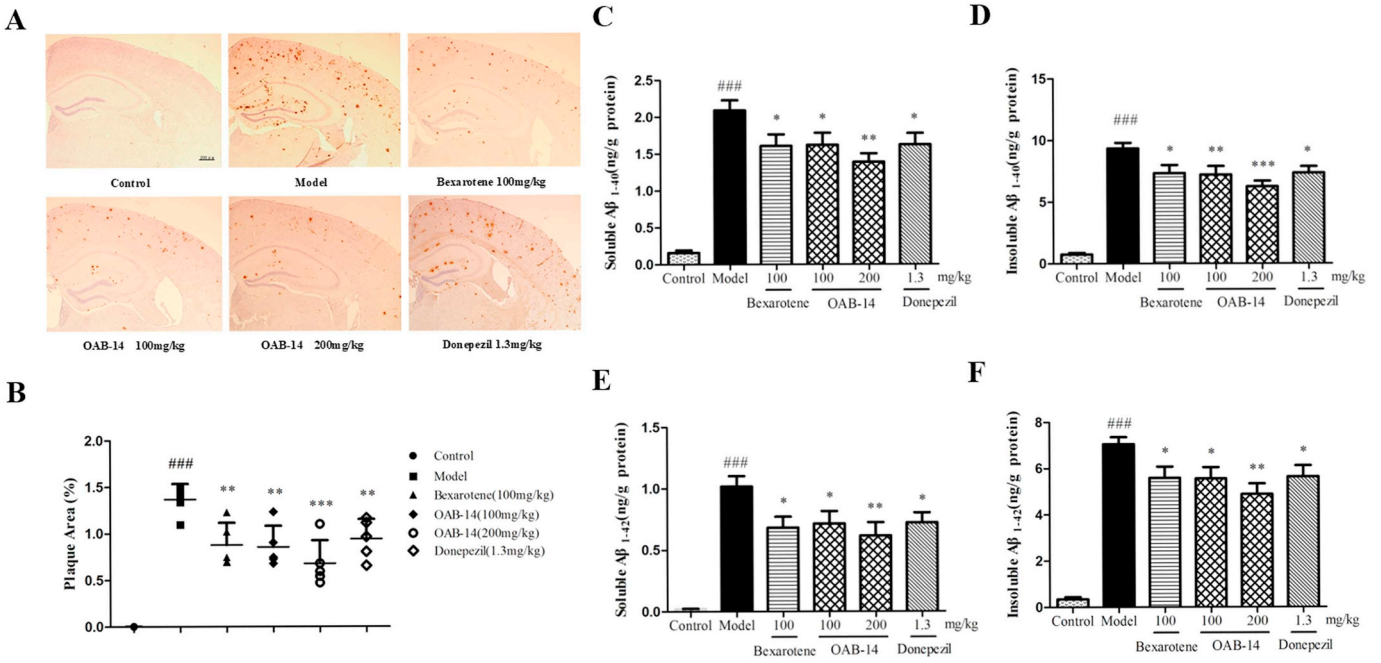

Fig. 6. OAB-14 clears Aβ in the cerebral cortex and hippocampus of APP/PS1 mice after chronic treatment. (A) Aβ immunostaining (6E10) in the brain of APP/PS1 transgenic mice. Scale bars, 200 μm. (B) Quantification of the Aβ plaque (6E10) area throughout the cerebral cortex and hippocampus of APP/PS1 transgenic mice. Levels of (C) soluble $A\beta_{1-40}$, (D) insoluble $A\beta_{1-40}$, (E) soluble $A\beta_{1-42}$ and (F) insoluble $A\beta_{1-42}$ in the cortex of APP/PS1 transgenic mice detected by ELISA. Data are presented as the mean ± SEM ($n = 5$). $^{###}p < 0.001$ vs. the control group and $^{*}p < 0.05$, $^{**}p < 0.01$ or $^{***}p < 0.001$ vs. the model group.

presenilin 1 (PS1) transgenic mice. Although its negative effects have been reported, bexarotene is currently the only drug that rapidly increases Aβ clearance. Therefore, we chose it as a positive control drug in our experiments. Since Aβ accumulation in the brains of patients with AD induces other pathological changes, such as tau hyperphosphorylation, neuronal loss, neuroinflammation and synaptic degeneration [15,16], we also investigated the effects of OAB-14 on these pathological events in AD and addressed its safety concerns.

2. Materials and methods

2.1. Small molecule design and synthesis

Small molecule design for the treatment of AD is a challenging issue due to the lack of clear AD pathology. As described above, bexarotene was able to clear Aβ in the brain. Tacrine hydrochloride hydrate is an inhibitor of both acetyl (AChE) and butyryl-cholinesterase (BChE) [17]. However, its application has been limited due to its liver toxicity. Based on the combination principle between tacrine and bexarotene, our group has designed and synthesized a series of compounds containing octamethyl octahydroanthracene, which was more liposoluble to pass the blood-brain barrier, and screened out the novel small molecule OAB-14 (Figs. 1 and S1).

The strategy adopted for the synthesis of OAB-14 is outlined in Fig. 2. The 2,5-dichloro-2,5-dimethylhexane **3** was obtained by chlorination with starting material 2,5-dimethylhexane-2,5-diol in the presence of Conc. HCl. 1,1,4,4,5,5,8,8-octamethyl-1,2,3,4,5,6,7,8-octahydroanthracene **4** was synthesized from intermediate **4** via Friedel-Crafts reaction. Then, the nitro compound **5** was prepared by direct nitration of **4**, which was reduced to the corresponding amine **6** by treatment with stannum powder and hydrochloric acid gas. Treatment **6** with 4-nitrobenzoyl chloride in refluxing xylene in the presence of DMAP and pyridine as a base, gave amide derivative **7**, which was reduced via 10% Pd/C and hydrogen to obtain intermediate **8**. The title compound was prepared in one-pot reaction from compound **8** and ethylenediamine in the presence of bis(trichloromethyl) carbonate and triethylamine with a purity of 97.79%. The positive control drug bexarotene was synthesized according to the literature [18] with a purity of 99.5%.

2.2. Mice

The APPswe/PS1Δe9 (APP/PS1) transgenic mice overexpress human APP with the Swedish double mutation (K595N and M596L) and the human presenilin 1 (PS1-dE9) mutant. APP/PS1 mice (8 months old, male) and C57BL/6 mice (8 months old, male) were purchased from the Beijing HFK Bioscience Co. Ltd. (Beijing, China). APP/PS1 mice were randomly divided into five groups and subjected to different treatment protocols (Table 1) and experimental schedules (Fig. 3A). C57BL/6 mice were used as the controls. APP/PS1 mice received treatments by oral gavage for 15 days (acute treatment from 8 to 8.5 months) using the T1 protocol and 90 days (chronic treatment from 8 to 11 months) using the T2 protocol. All experimental procedures using animals were performed according to the Guide for the Care and Use of Laboratory Animals (Permit Number: SYPU-IACUC-S2015.03.04-101).

2.3. Novel object recognition (NOR) test

Rodents display a natural tendency to investigate a novel object instead of a familiar one [19]. The NOR test was performed from days 6 to 9 after drug administration. The method is described in our previous study [20]. The experimental apparatus consisted of a wooden square box (45 cm long × 15 cm tall × 45 cm wide). First, in the habituation phase (two days), the mice were placed in the empty box to adapt to the environment for 5 min. In the training phase (two days), two identical objects A1 and A2 were placed in the box. Each mouse was placed in the box to freely explore the objects for 5 min, and the total time the mouse spent exploring the objects was recorded. The test phase began 1 h after training, and the mouse was placed back in the box with object A1 and a novel object B for 5 min. The total time the mouse spent exploring objects A1 (tA1) and B (tB) was recorded. The preferential index was

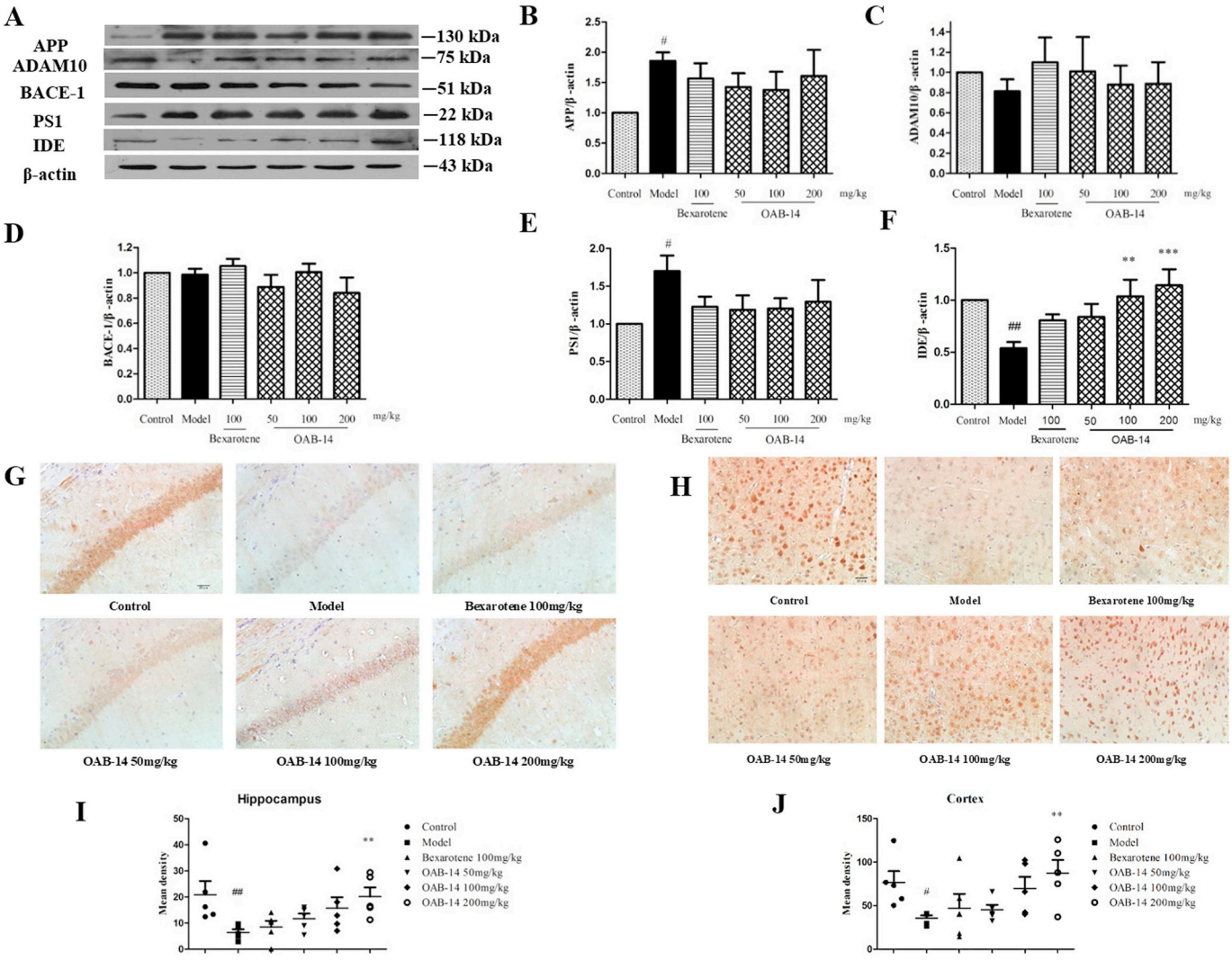

Fig. 7. OAB-14 does not change Aβ generation-related proteins expression, but increases Aβ-degrading enzyme expression in the cortex and hippocampus of APP/PS1 transgenic mice after acute treatment. (A) Western blot in the cortex of APP/PS1 transgenic mice. (B–F) Quantification of (B) APP, (C) ADAM10, (D) BACE-1, (E) PS1, and (F) IDE protein expression by Western blot. Images showing NEP immunostaining in (G) hippocampus and (H) cortex of APP/PS1 mice. Scale bars, 20 μm. Quantification of the mean density of NEP in the (I) hippocampus and (J) cortex of APP/PS1 transgenic mice. Data are presented as the mean ± SEM ($n = 5$). $^{\#}p < 0.05$ or $^{\#\#}p < 0.01$ vs. the control group and $^{**}p < 0.01$ or $^{***}p < 0.001$ vs. the model group.

calculated using the following equation: Preferential index (%) at 1 h = tB/(tA1 + tB) × 100%.

2.4. Morris water maze (MWM) test

The MWM test was performed from day 11 to day 15 after drug administration as described in our previous study [21]. The MWM consisted of a large pool (100 cm in diameter, 40 cm tall, filled with water at 23 ± 1 °C). A small white platform (10 cm in diameter) was submerged 1 cm below the surface of the water.

2.5. Nest building test

Each mouse was placed in single cages containing corn crumbs for one week. The method was implemented using a previously reported protocol [22]. One piece of cotton (5 × 5 cm) was placed in each cage as nesting material. The nest building behaviour was rated 12 h later on a 5-point scale from 1 to 5 as follows: 1 = not noticeably touched; 2 = partially torn up; 3 = mostly shredded, but often no identifiable nest site; 4 = identifiable but flat nest, and 5 = perfect or nearly perfect nest.

2.6. Analysis of immunohistochemical and immunofluorescence staining using confocal microscopy

After the behavioural test, mice were anaesthetised and intracardially perfused with saline (0.9%) followed by ice-cold 4% paraformaldehyde in PBS. The brains were post-fixed with 4% paraformaldehyde overnight at 4 °C, embedded in paraffin, and then cut into 4-μm-thick sections. For Aβ and neprilysin (NEP) immunohistochemical staining, sections were incubated with anti-Aβ antibody (6E10, SIG-39320, Covance) and anti-NEP antibody (bs-2402R, Bioss) overnight at 4 °C. After rinsing, the sections were incubated with secondary antibody (Santa Cruz) for 30 min at 37 °C. Sections were incubated with avidin-biotin enzyme reagent (Santa Cruz), and the positive signal was visualized using DAB. The plaque area and NEP density in each section were analysed using an Olympus IX 71 microscope and quantified using the Image-Pro Plus 6.0 software.

For NeuN immunofluorescence staining, the sections were incubated with a rabbit anti-NeuN antibody (ab177487, Abcam) overnight at 4 °C. After rinsing, the sections were incubated with Cy3-conjugated Affinipure goat anti-rabbit lgG (Proteintech) for 1 h at 37 °C. The immunofluorescence staining was observed and images were

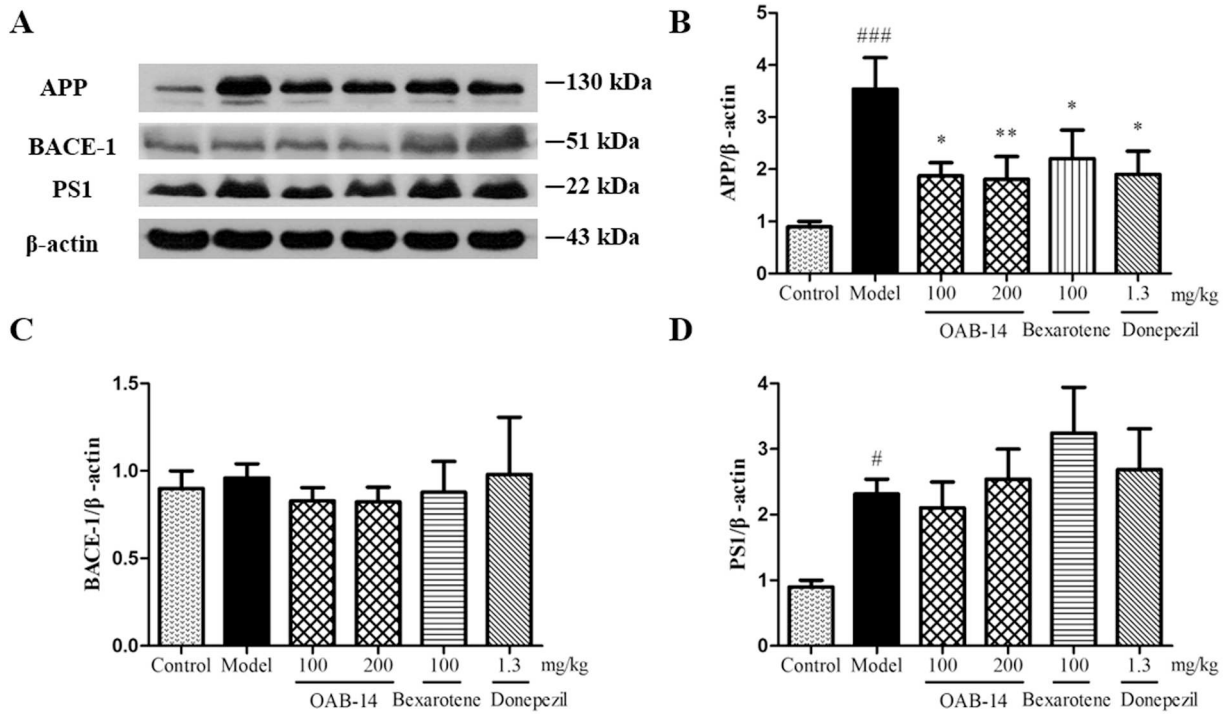

Fig. 8. OAB-14 does not change Aβ generation-related protein expression in the cortex of APP/PS1 transgenic mice after chronic treatment. (A) Representative Western blots. (B–D) Quantification of (B) APP, (C) BACE-1, and (D) PS1 protein expression. Data are presented as the mean ± SEM ($n = 5$) $^{\#}p < 0.05$ or $^{\#\#\#}p < 0.001$ vs. the control group and $^{*}p < 0.05$ or $^{**}p < 0.01$ vs. the model group.

captured using a laser scanning confocal microscope (Nikon C-2 Plus, Tokyo, Japan).

For double immunofluorescence staining, sections were incubated with rabbit anti-Iba1 (ab178846, Abcam) and mouse anti-Aβ (6E10, Covance) or mouse anti-CD36 (NB110-59724, Novus) antibodies overnight at 4 °C. After washing, the sections were incubated with a mixture of fluorescein (FITC)-conjugated Affinipure goat anti-mouse lgG and Cy3-conjugated Affinipure goat anti-rabbit lgG (Proteintech) for 1 h at 37 °C. The immunofluorescence staining was observed and images were captured using a laser scanning confocal microscope (Nikon C-2 Plus, Tokyo, Japan).

2.7. Thioflavin S fluorescence staining

Paraffin sections were dewaxed and then washed. Peroxidase blockers were added and incubated for 10 min, then rinsed with PBS. The sections were incubated with a thioflavin S (T1892, Sigma) ethanol solution in the dark for 10 min. After washing, the sections were mounted in a water-soluble mounting medium. Images were acquired with an Olympus IX71 inverted fluorescence microscope.

2.8. ELISA of $A\beta_{1-40}$ and $A\beta_{1-42}$ levels

The levels of $A\beta_{1-40}$ and $A\beta_{1-42}$ in the mouse brain were determined using the Colorimetric BetaMark x-40 (Biolegend, No.:842301) and x-42 ELISA kits (Biolegend, No.:842401). After the behavioural test, the entire cortex and hippocampus was dissected and store at −80 °C. The cortex was homogenized in 2% SDS-PBS (0.01 M) containing protease inhibitors (Biosharp) and then ultracentrifuged (350,000*g*, 20 min). The supernatant was utilized to measure soluble $A\beta_{1-40}$ or $A\beta_{1-42}$ levels with ELISAs, according to the manufacturer's specifications. The pellet was homogenized in 1% Triton-PBS (0.01 M) containing protease inhibitors (Biosharp). The method used to process the homogenate was the same as described above. The supernatant was subjected to ELISAs to measure the levels of insoluble $A\beta_{1-40}$ or $A\beta_{1-42}$.

2.9. Western blot analysis

The protein (30 μg) was separated on 12% gradient SDS-PAGE gels and electrophoretically transferred to 0.45-μm polyvinyl difluoride (PVDF) membranes (Millipore, MA, USA). Membranes were blocked with 5% skim milk in PBS for 2 h at room temperature and then incubated with primary antibodies overnight at 4 °C. After washing, the membranes were incubated with secondary antibodies (Santa Cruz) for 2 h at room temperature. The immunoreactive bands were visualized using an ECL Western blotting kit (Kangwei, China). The intensity of the immunoblotted bands was quantified by densitometry using the Quantity One 4.6.2 software (Bio-Rad, Hercules, CA, USA) and normalized to the β-actin levels in the corresponding sample. The results are expressed as relative percentages to the control. The following primary antibodies were used: anti-ApoE (sc-17750, Santa Cruz), anti-ApoE3 (bs-5039R, Bioss), anti-ApoE4 (bs-5038R, Bioss), anti-ABCA1 (NB400-105, Novus), anti-ABCG1 (NB400-132, Novus), anti-IDE (21728-1-AP, Proteintech), APP (2452S, CST), BACE1 (bs-0164R, Bioss), PS1 (5643P, CST), ADAM10 (BS60338, Bioworld), anti-ARG I (ab124917, Abcam), anti-iNOS (ab178945, Abcam), anti-IL-1β (16806-1-AP, Proteintech), anti-IL-6 (21865-1-AP, Proteintech), anti-TNF-α (9427, CST), anti-SYP (sc-17750, Santa Cruz), anti-GAP43 (sc-17790, Santa Cruz), anti-PSD95 (ab18258, Abcam), anti-Nogo-A (sc-25660, Santa Cruz), anti-NeuN (ab177487, Abcam), anti-acetylated H3 (Lys9; clone C5B11) (9649P, CST), anti-H3 (17168-1-AP, Proteintech), anti-BDNF (ab108319, Abcam), anti-TrkB (phospho Y515, ab109684, Abcam), anti-TrkB (13129-1-AP, Proteintech), anti-p-Raf (9427, CST), anti-Raf (51140-1-AP, Proteintech), anti-ERK1/2 (16443-1-AP, Proteintech), anti-p-ERK1/2 (ab76299, Abcam), anti-p-Tau-Thr231 (44-746G, Invitrogen), anti-p-Tau-Ser404 (44-758G, Invitrogen), anti-p-Tau-Ser396 (sc-101815, Santa Cruz), anti-Tau-5 (AHB0042, Invitrogen), anti-p-GSK3β-Tyr216 (sc-135653, Santa Cruz), anti-GSK-3β (bs-0028R, Bioss), anti-p-PI3K-Tyr458 (p85) (4228p, CST), anti-PI3K (p110β) (bs-6423R, Bioss), anti-p-AKT (sc-7985, Santa Cruz), anti-AKT1/2 (N-19) (sc-1619, Santa Cruz), anti-Wnt-3α (WL0199a, Wanlei),

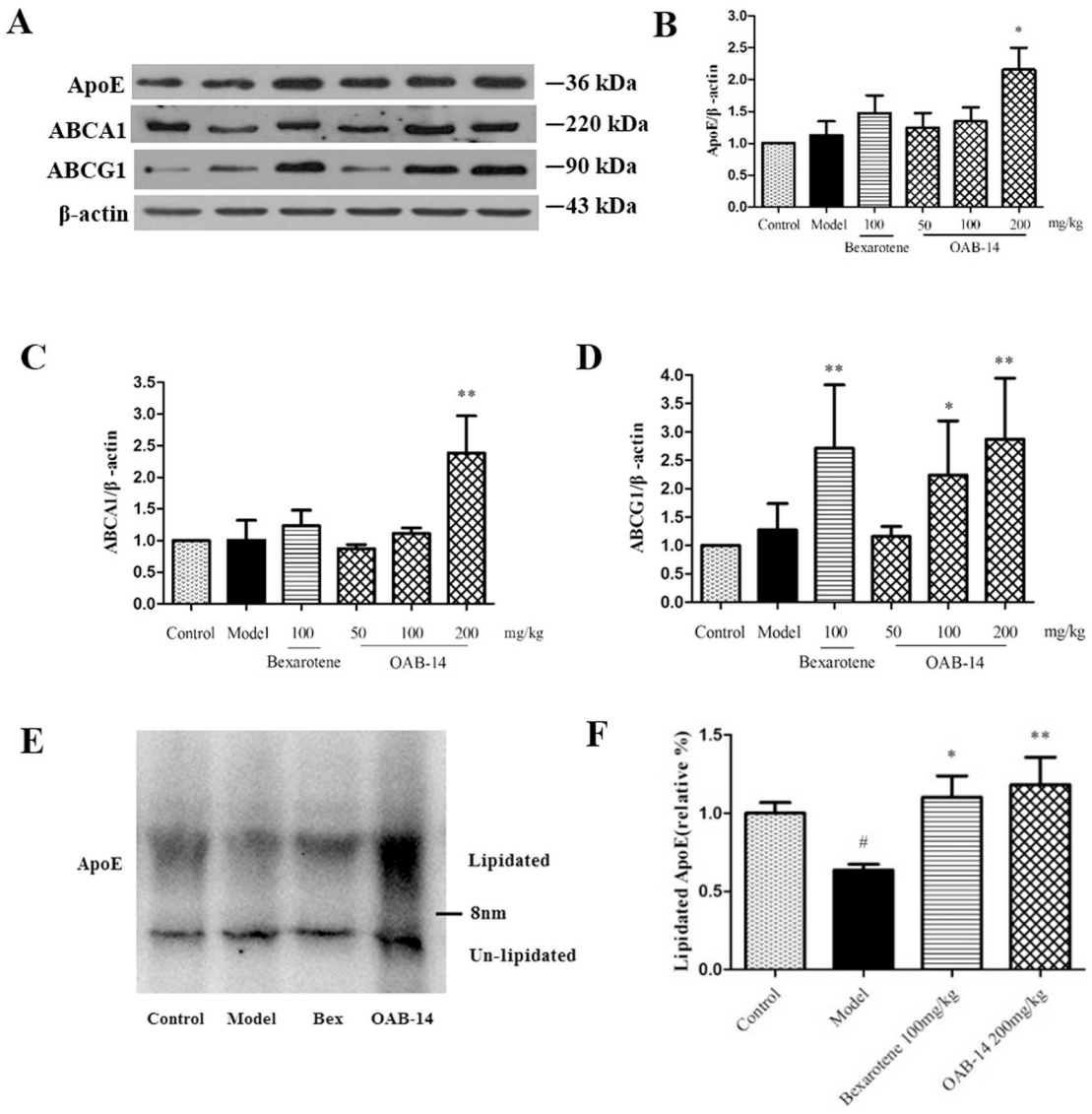

Fig. 9. OAB-14 increases ApoE, ABCA1, ABCG1 and lipidated ApoE expression in the cortex of APP/PS1 transgenic mice. (A) Representative Western blot in the cortex of APP/PS1 transgenic mice. (B–D) Quantification of (B) ApoE, (C) ABCA1, and (D) ABCG1 protein expression. (E) Native gel electrophoresis blot. (F) Quantification of blot for lipidated ApoE expression. Data are presented as the mean ± SEM ($n = 5$). $^{\#}p < 0.05$ vs. the control group and $^{*}p < 0.05$ or $^{**}p < 0.01$ vs. the model group.

anti-p-PP2A (Y307) (ab32104, Abcam), anti-PP2A-Cα/β (L-307) (sc-14020, Santa Cruz) and anti-β-actin (sc-47778, Santa Cruz).

Native gel electrophoresis was used to measure the amount of lipidated ApoE [10]. The mice cortices were lysed immediately following homogenization, and then briefly centrifuged to remove the debris. Proteins (34 μg of protein per lane) were separated on a 12% gradient native-PAGE gels at 90 V for 3 h. Then, the gels were electrophoretically transferred to 0.45-μm PVDF membranes (Millipore, MA, USA). The lipidated and unlipidated ApoE bands were naturally separated at 8 nm, with bands larger than 8.0 nm considered as lipidated ApoE [23].

2.10. Transmission electron microscopy of neurons and synapses

The mice were anaesthetised and intracardially perfused with saline (0.9%) followed by perfusion fluid containing 4% paraformaldehyde and 2.5% glutaraldehyde in 0.01 M PBS (pH = 7.4). The hippocampi were isolated and post-fixed with 2.5% glutaraldehyde. After washing, the hippocampi were fixed, washed, dehydrated, and then embedded in Epon 812 (TAAB Laboratories Equipment Ltd., Berkshire, England). After locating the CA1 region of the hippocampus, the serial sections were sliced at a thickness of 70 nm using an ultramicrotome, double stained with 3% uranium acetate-lead citrate, and then observed under a transmission electron microscope (Hitachi H-7650, Tokyo, Japan).

2.11. The liver index

After acute and chronic treatment, the body weight of mice was measured, and the livers were immediately removed and weighed. Calculations were performed according to the following equation: Liver index (%) = liver weight/body weight × 100%.

2.12. Acute toxicity experiment

Forty C57 mice were randomly divided into the control group and the OAB-14 group. Each group comprised 10 female mice and 10 male mice. The OAB-14 group received a single oral administration of 4 g/kg OAB-14, and the control group was orally administered the same volume of vehicle. The body weights, toxic reactions, and the death of the mice were continuously observed for 14 days.

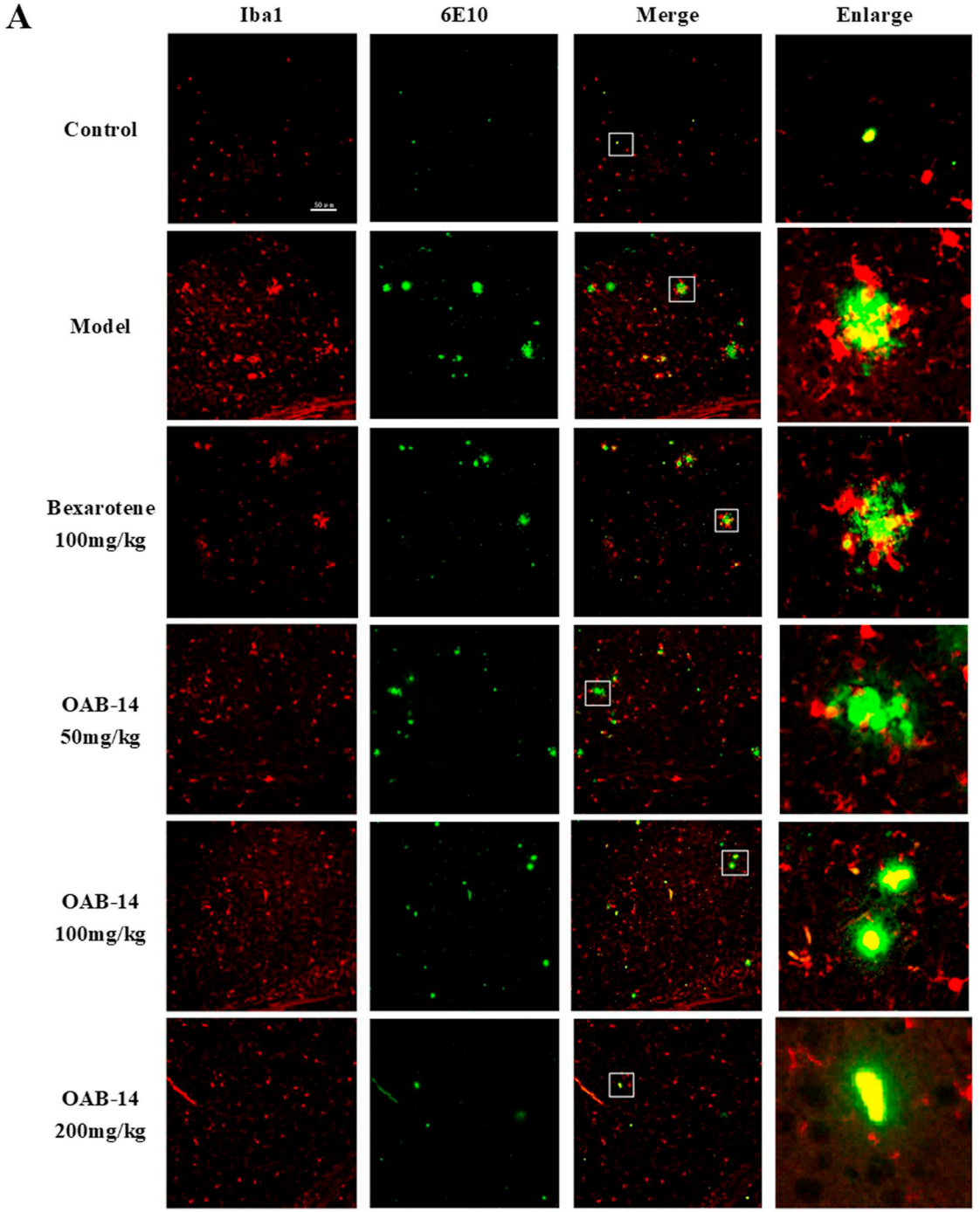

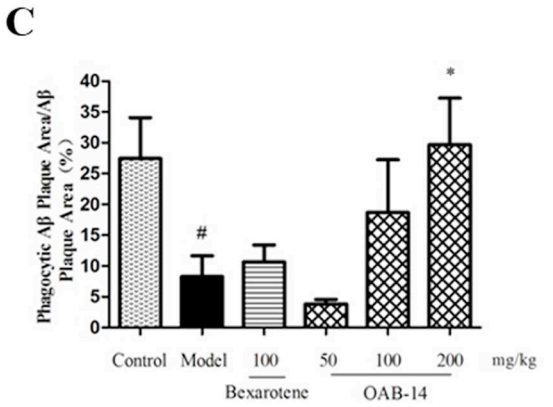

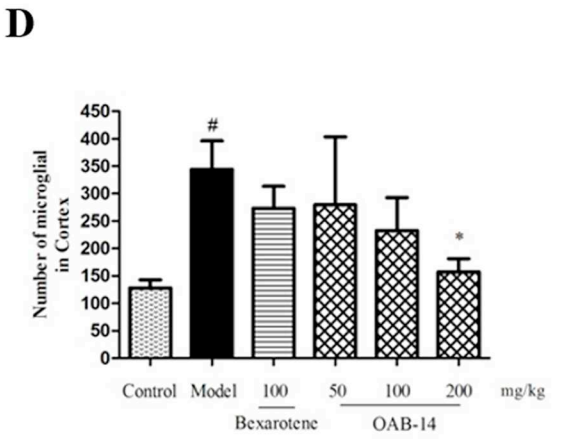

Fig. 10. OAB-14 promotes microglia phagocytosis Aβ in the cortex and hippocampus of APP/PS1 transgenic mice. Microglia phagocytosis Aβ in the (A) cortex and (B) hippocampus of APP/PS1 mice. Scale bars, 20 μm. Red: Iba1. Green: Aβ. The percentage of phagocytic Aβ plaque areas to Aβ plaque areas in the (C) cortex or (E) hippocampus. The number of activated microglia in the (D) cortex or (F) hippocampus. Data are presented as the mean ± SEM ($n = 5$). $^{\#}p < 0.05$ or $^{\#\#\#}p < 0.001$ vs. the control group and $^{*}p < 0.05$ or $^{**}p < 0.01$ vs. the model group.

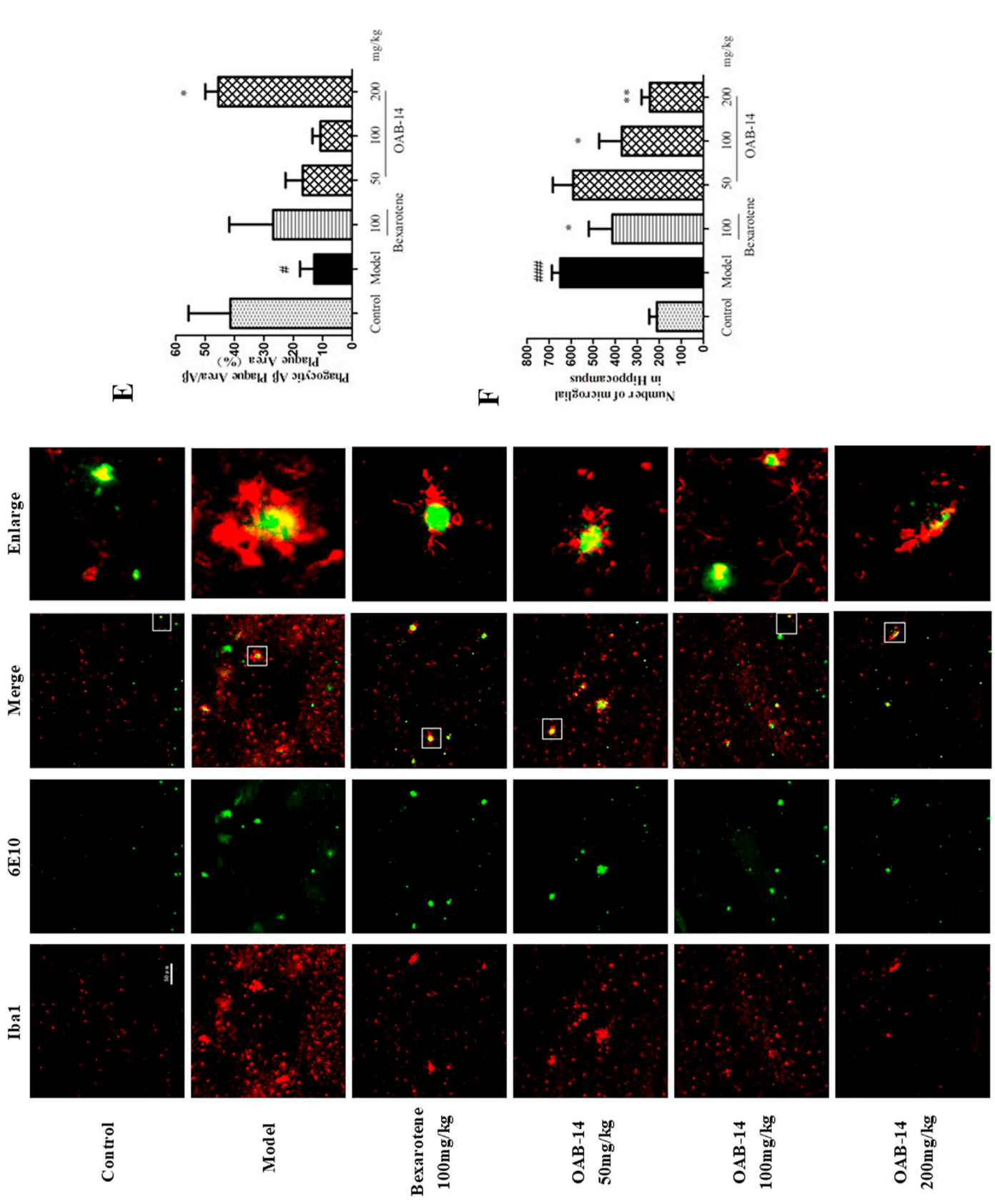

Fig. 10. (*continued*)

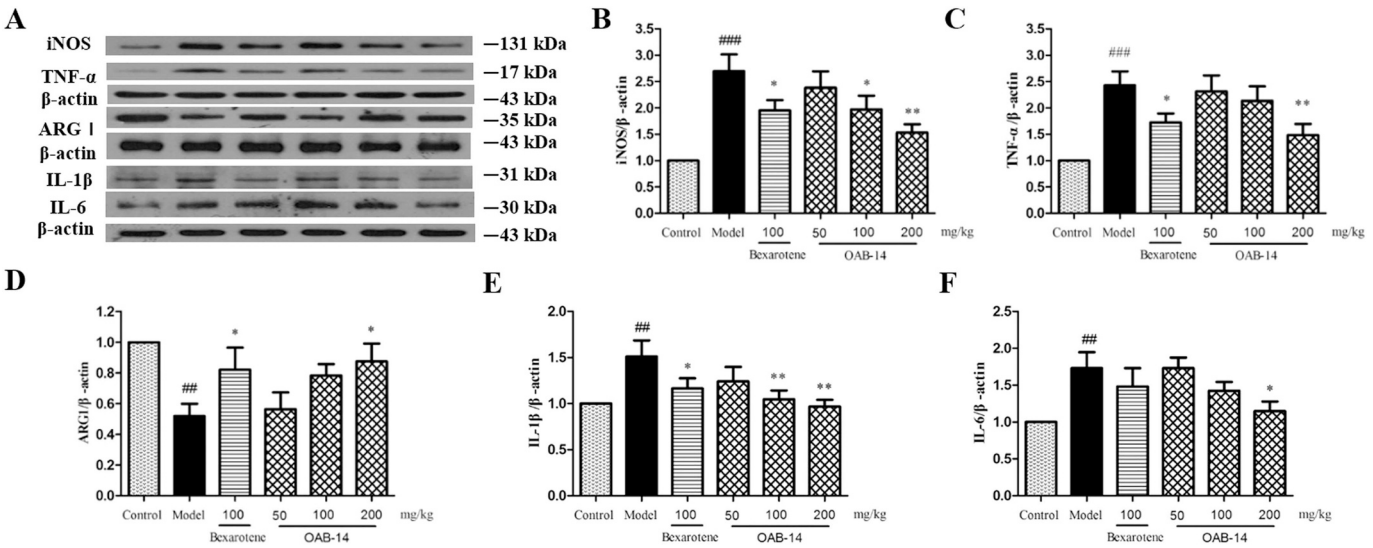

Fig. 11. OAB-14 stimulates the transformation of microglia from M1 to M2 in the brain of APP/PS1 mice. (A) Representative Western blot. (B–F) Quantification of (B) iNOS (M1 marker), (C) TNF-α, (D) ARGI (M2 marker), (E) IL-1β, and (F) IL-6 protein expression. Data are presented as the mean ± SEM ($n = 5$). $^{\#\#}p < 0.01$ or $^{\#\#\#}p < 0.001$ vs. the control group and $^{*}p < 0.05$ or $^{**}p < 0.01$ vs. the model group.

2.13. Colocalization analysis

The colocalization analyses used the ImageJ 1.50i software.

2.14. Statistical analysis

All data are expressed as the mean ± standard error of the mean (SEM), and statistical analyses were conducted with one-way ANOVA using SPSS 16.0. The exact F statistic value and degrees of freedom were used to calculate probabilities, and the results were considered statistically significant if $p < 0.05$. Data from the MWM tests were analysed using two-way ANOVA.

3. Results

3.1. OAB-14 improves cognitive impairments in APP/PS1 mice

The preferential index was used to evaluate image discrimination memory in the NOR test. In the training phase, each group of mice spent similar amounts of time exploring the two identical objects, indicating that mice had no bias towards either of them. In the test phrase, the exploration time for the new object was dramatically decreased in the model group compared to the control group ($F_{5,49} = 3.630$, $p = 0.007$; post hoc, $p = 0.001$; Fig. 3B). In contrast, OAB-14 (100 and 200 mg/kg) treated APP/PS1 mice showed a strong preference for the novel object B ($p = 0.33$ for 100 mg/kg, $p = 0.01$ for 200 mg/kg; Fig. 3B). The MWM test was used to evaluate spatial memory by monitoring the swimming distance travelled to reach the platform. During the training phase, the performance of the six groups differed significantly ($F_{group} = 10.875$, $p = 0.000$; $F_{day} = 189.166$, $p = 0.000$; $F_{group \times day} = 1.286$, $p = 0.214$, Fig. 3C). In particular, the APP/PS1 mice exhibited a significant increase in swimming distance on day 4, indicating deficits in spatial memory ($F_{5,49} = 2.443$, $p = 0.047$; post hoc test, $p = 0.003$; Fig. 3C), whereas the deficit was significantly improved by OAB-14 treatment (200 mg/kg) in APP/PS1 mice ($p = 0.035$; Fig. 3C). In the probe test, OAB-14 (200 mg/kg) treated mice swam a longer distance in the target quadrant than APP/PS1 mice (Fig. 3D). Nest building is a typical social behaviour of mice, and APP/PS1 mice displayed a significantly impaired nesting ability ($F_{5,60} = 8.867$, $p = 0.000$; post hoc test, $p = 0.000$; Fig. 3E); however, OAB-14 remarkably restored the nesting ability in APP/PS1 mice at 12 h ($p = 0.000$ for 100 mg/kg, $p = 0.000$ for 200 mg/kg; Fig. 3E). The observed improvements in behaviours were also recapitulated in mice subjected to chronic treatment (Fig. 4A–D).

3.2. OAB-14 clears Aβ from the cerebral cortex and hippocampus of APP/PS1 mice

Total Aβ and fibrotic Aβ levels, which were labelled with the anti-Aβ antibody (6E10) (Fig. 5A) and thioflavin S (Fig. 5C), respectively, were used to evaluate the effect of OAB-14 on Aβ deposition. There were more Aβ deposits in the cerebral cortex and hippocampus of APP/PS1 mice than in the control mice. After acute treatment with OAB-14 200 mg/kg, the total Aβ levels ($F_{5,24} = 15.958$, $p = 0.000$; post hoc test, $p = 0.000$; Fig. 5B) and fibrotic Aβ plaques ($F_{5,24} = 15.818$, $p = 0.000$; post hoc test, $p = 0.000$; Fig. 5D) in the cerebral cortex and hippocampus of APP/PS1 mice were reduced to 29% and 33%, respectively. Meanwhile, ELISA revealed that the levels of soluble $Aβ_{1–40}$ and $Aβ_{1–42}$, and insoluble $Aβ_{1–40}$ and $Aβ_{1–42}$ in the cerebral cortex of APP/PS1 mice were significantly reduced compared to those in the model group (soluble $Aβ_{1–40}$ $F_{5,24} = 5.487$, $p = 0.002$; post hoc test, $p = 0.005$; soluble $Aβ_{1–42}$ $F_{5,24} = 8.726$, $p = 0.000$; post hoc test, $p = 0.001$; insoluble $Aβ_{1–40}$ $F_{5,24} = 9.712$, $p = 0.000$; post hoc test, $p = 0.004$; insoluble $Aβ_{1–42}$ $F_{5,24} = 10.486$, $p = 0.000$; post hoc test, $p = 0.017$; Fig. 5E–H), which is consistent with the thioflavin S and 6E10 immunohistochemical staining. Based on these results, OAB-14 effectively reduced Aβ levels in APP/PS1 mice after acute treatment. We also tested the effect of chronic OAB-14 treatment on Aβ levels in the brains of APP/PS1 mice. The results were consistent with the findings for the acute treatment (Fig. 6).

Aβ levels in the brain are reduced through the following two mechanisms: decreased Aβ production or increased Aβ clearance. We first investigated Aβ production. Interestingly, the levels of APP and enzymes responsible for generating Aβ, ADAM10, BACE-1, PS1, etc., were unchanged after acute (APP $F_{5,24} = 1.205$, $p = 0.337$; ADAM10 $F_{5,24} = 0.247$, $p = 0.937$; BACE-1 $F_{5,24} = 1.164$, $p = 0.355$; PS1 $F_{5,24} = 1.629$, $p = 0.191$; Fig. 7B–E) and chronic OAB-14 treatment (except for APP) (Fig. 8B–D). However, the levels of the Aβ-degrading enzymes NEP and IDE were significantly increased by acute treatment in APP/PS1 mice (NEP in the hippocampus $F_{5,24} = 3.197$, $p = 0.024$; post hoc test, $p = 0.008$; in the cortex $F_{5,24} = 2.821$, $p = 0.038$; post hoc test, $p = 0.006$; IDE $F_{5,24} = 3.819$, $p = 0.011$; post hoc test, $p = 0.001$; Fig. 7F–J). Alternatively, in our experiment, the RXR agonist bexarotene had no effect on NEP and IDE levels, which is consistent

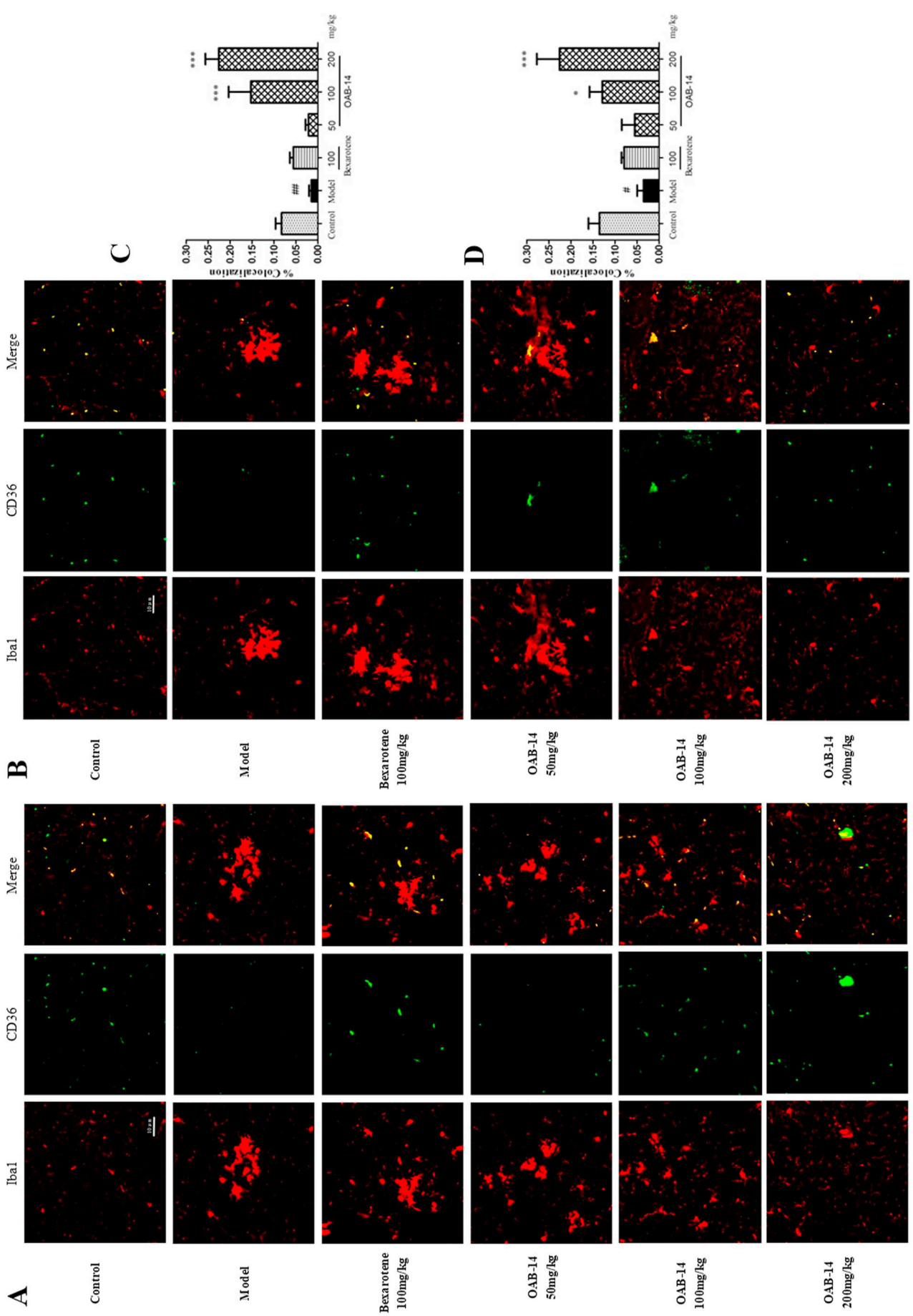

Fig. 12. OAB-14 enhances the expression of CD36 on the surface of microglia in the brain of APP/PS1 mice. (A and B) Immunostaining of CD36 on the surface of microglia in the (A) cortex and (B) hippocampus of APP/PS1 mice. Scale bars, 10 μm. Red: Iba1. Green: CD36. (C) Colocalization in the cortex. (D) Colocalization in the hippocampus. Data are presented as the mean ± SEM ($n = 5$). $^{\#}p < 0.05$ or $^{\#\#}p < 0.01$ vs. the control group and $^{*}p < 0.05$ or $^{***}p < 0.001$ vs. the model group.

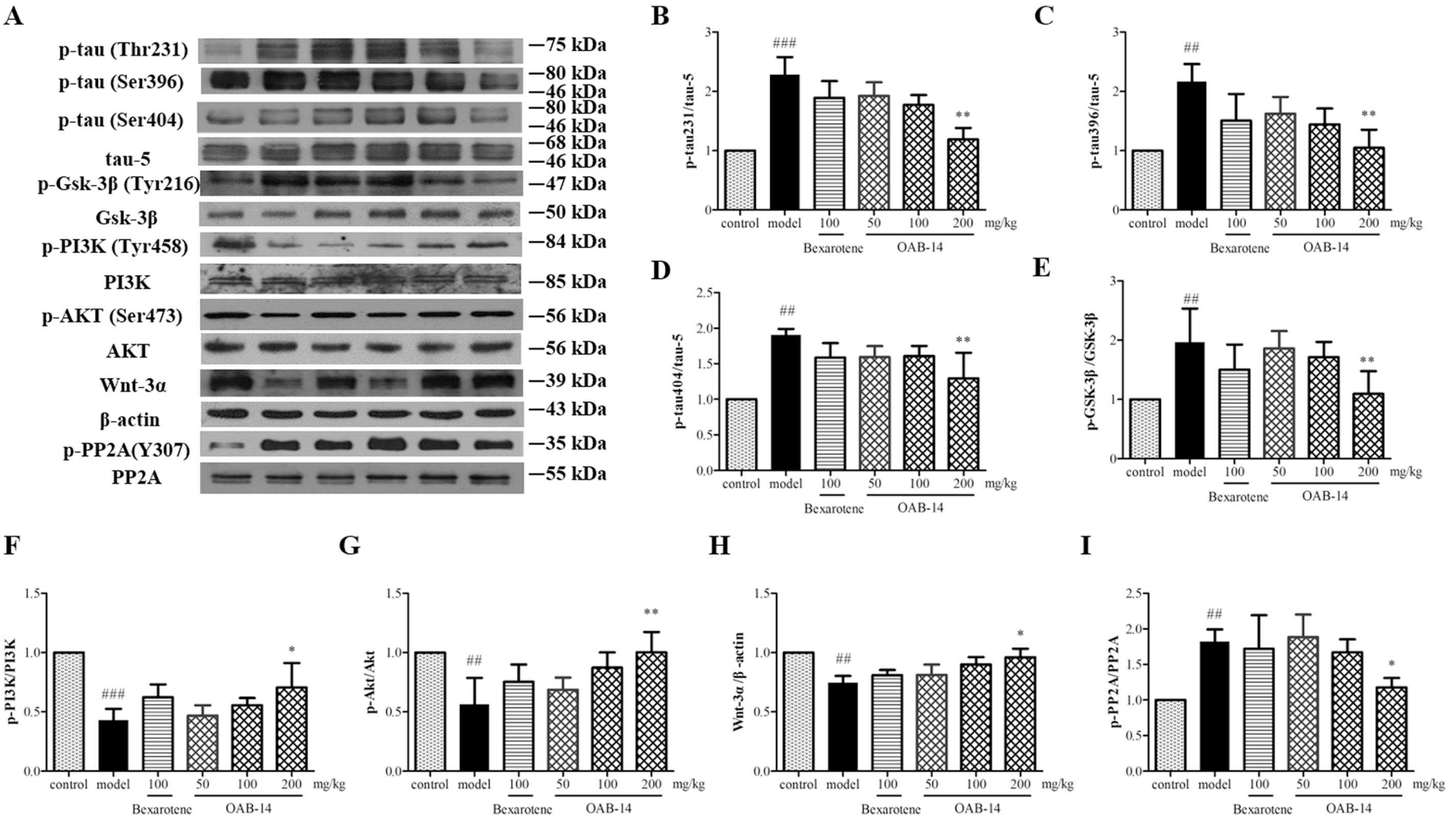

Fig. 13. OAB-14 decreases tau-hyperphosphorylation in the cerebral cortex of APP/PS1 transgenic mice. (A) Representative Western blot. Quantitative analysis for (B) pThr231-tau, (C) pSer396-tau, (D) p-Ser404, (E) p-GSK3β(Tyr216) and total GSK3β, (F) p-PI3K(Tyr458) and total PI3K, (G) p-AKT(Ser473) and total AKT, (H) Wnt-3α, and (I) p-PP2A(Y307) and total PP2A ($n = 5$). Data are presented as the mean ± SEM. $^{\#\#}p < 0.01$ or $^{\#\#\#}p < 0.001$ vs. the control group and $^{*}p < 0.05$ or $^{**}p < 0.01$ vs. the model group.

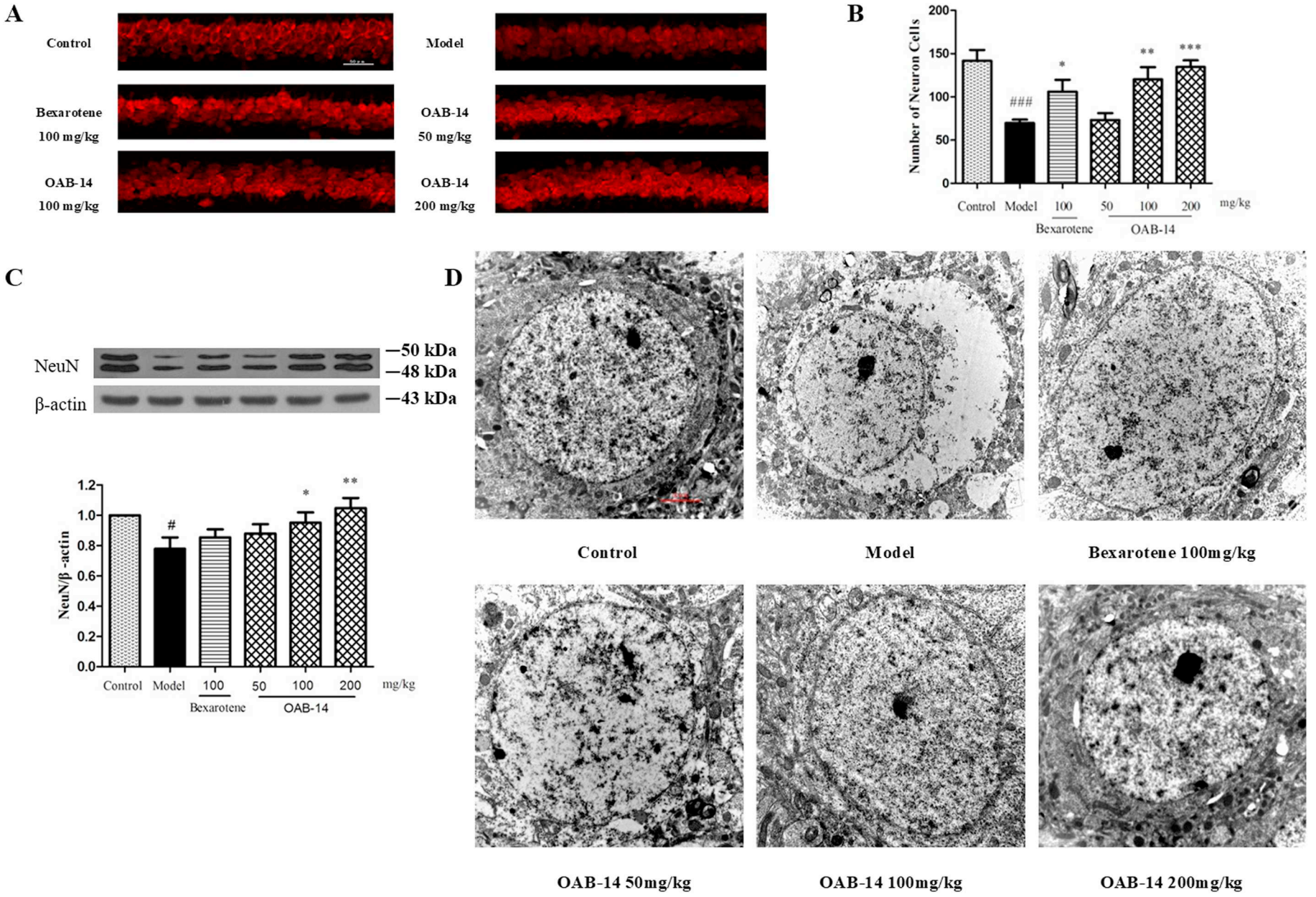

Fig. 14. OAB-14 repairs neuronal loss in the hippocampus of APP/PS1 transgenic mice. (A) Immunofluorescence of NeuN ($n = 5$). Scale bars, 50 μm. (B) Quantification of the number of NeuN cells. (C) Western blot and quantitative analysis for NeuN ($n = 5$). (D) The ultrastructure of neuronal nuclei in the CA1 area of the hippocampus by transmission electron microscopy ($n = 3$, ×10,000, 2 μm). Data are presented as the mean ± SEM. $^{\#}p < 0.05$ or $^{\#\#\#}p < 0.001$ vs. the control group and $^{*}p < 0.05$, $^{**}p < 0.01$ or $^{***}p < 0.001$ vs. the model group.

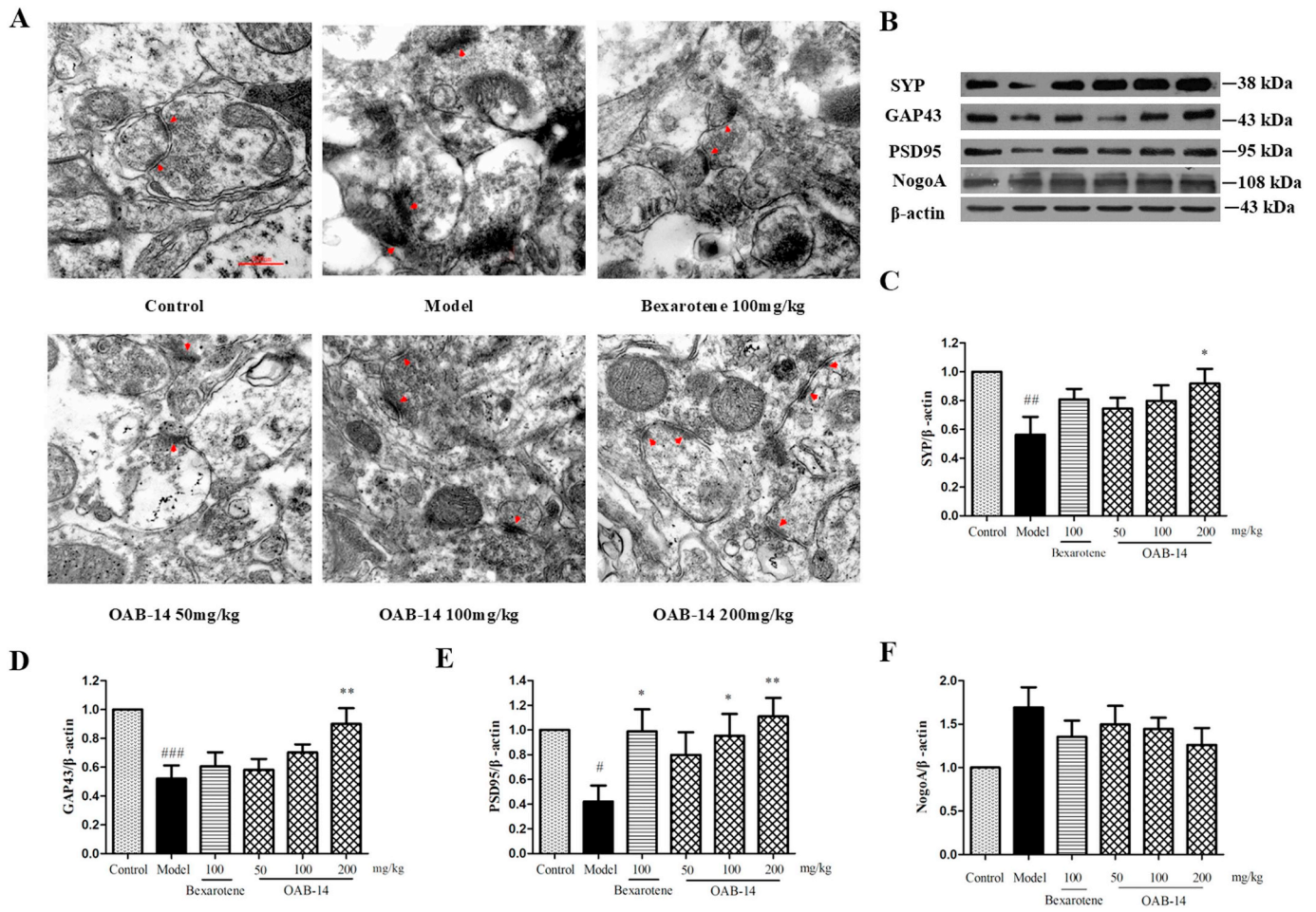

Fig. 15. OAB-14 improves synaptic structure and increases the expression of synapse related proteins. (A) The ultrastructure of the synapses in the CA1 area of the hippocampus by transmission electron microscopy. (n = 3, ×40,000, 500 nm) (B) Representative Western blot. Quantification of (C) SYP, (D) GAP43, (E) PSD95, and (F) Nogo A protein expression (n = 5). Data are presented as the mean ± SEM $^{\#}p < 0.05$, $^{\#\#}p < 0.01$ or $^{\#\#\#}p < 0.001$ vs. the control group and $^{*}p < 0.05$ or $^{**}p < 0.01$ vs. the model group.

with the findings of a previous study [10]. Therefore, we postulated that the acute OAB-14-induced reduction in Aβ levels in the brain might be achieved by increasing Aβ clearance, rather than reducing Aβ generation. Thus, we then examined the effect of OAB-14 on the ApoE pathway, which is the main mechanism by which bexarotene induces Aβ clearance. Acute treatment with OAB-14 at 200 mg/kg increased the protein-expression of ApoE, ATP-binding cassette transporter A1 (ABCA1) and G1 (ABCG1), and then elevated the levels of lipidated ApoE in APP/PS1 mice (ApoE $F_{5,24} = 2.684$, $p = 0.046$; post hoc test, $p = 0.006$; ABCA1 $F_{5,24} = 3.606$, $p = 0.014$; post hoc test, $p = 0.003$; ABCG1 $F_{5,24} = 6.788$, $p = 0.000$; post hoc test, $p = 0.002$; lipidated ApoE $F_{3,16} = 4.172$, $p = 0.023$; post hoc test, $p = 0.005$; Fig. 9B–F), which might be another mechanism by which OAB-14 clears soluble Aβ from the brain.

Immunostaining showed that OAB-14 treatment promoted microglia-mediated phagocytosis of Aβ in the cortex ($F_{5,24} = 2.656$, $p = 0.048$; post hoc test, $p = 0.028$) and hippocampus ($F_{5,24} = 2.650$, $p = 0.048$; post hoc test, $p = 0.019$; Fig. 10A–C, E) and reduced the number of Iba1-labelled activated microglia in the cortex ($F_{5,24} = 2.800$, $p = 0.040$; post hoc test, $p = 0.012$) and hippocampus ($F_{5,24} = 5.255$, $p = 0.002$; post hoc test, $p = 0.001$; Fig. 10D, F). The expression of a marker of the proinflammatory M1 phenotype, iNOS, was substantially decreased by acute treatment with OAB-14 ($F_{5,24} = 6.461$, $p = 0.001$; post hoc test, $p = 0.002$; Fig. 11B). Conversely, the expression of arginase I (ARG I), a marker of the anti-inflammatory M2 phenotype, was significantly increased ($F_{5,24} = 3.551$, $p = 0.015$; post hoc test, $p = 0.017$; Fig. 11D), accompanied by decreased levels of the inflammatory cytokines IL-1β, IL-6, and TNF-α (IL-1β $F_{5,24} = 2.997$, $p = 0.031$; post hoc test, $p = 0.003$; IL-6 $F_{5,24} = 3.374$, $p = 0.019$; post hoc test, $p = 0.018$; TNF-α $F_{5,24} = 5.710$, $p = 0.001$; post hoc test, $p = 0.008$; Fig. 11C, E, and F), suggesting that OAB-14 stimulated the transformation of microglia from classically activated macrophages (M1) to alternatively activated macrophages (M2).

3.3. OAB-14 increases CD36 expression on the surface of microglia in the brains of APP/PS1 mice

We analysed the localization of CD36 staining in microglia to examine the expression of CD36 on the surface of microglia. The model group exhibited lower colocalization than the control group (in the cortex $F_{5,24} = 29.863$, $p = 0.000$; post hoc test, $p = 0.003$; in the hippocampus $F_{5,24} = 4.701$, $p = 0.004$; post hoc test, $p = 0.036$; Fig. 12). After acute treatment with OAB-14, there was a remarkable increase in colocalization compared to the model group (in the cortex $p = 0.000$ for 100 mg/kg and 200 mg/kg; in the hippocampus $p = 0.049$ for 100 mg/kg, $p = 0.000$ for 200 mg/kg; Fig. 12C and D). In contrast, the bexarotene-treated group did not present any changes in the colocalization (in the cortex $p = 0.056$; in the hippocampus $p = 0.339$; Fig. 12C and D).

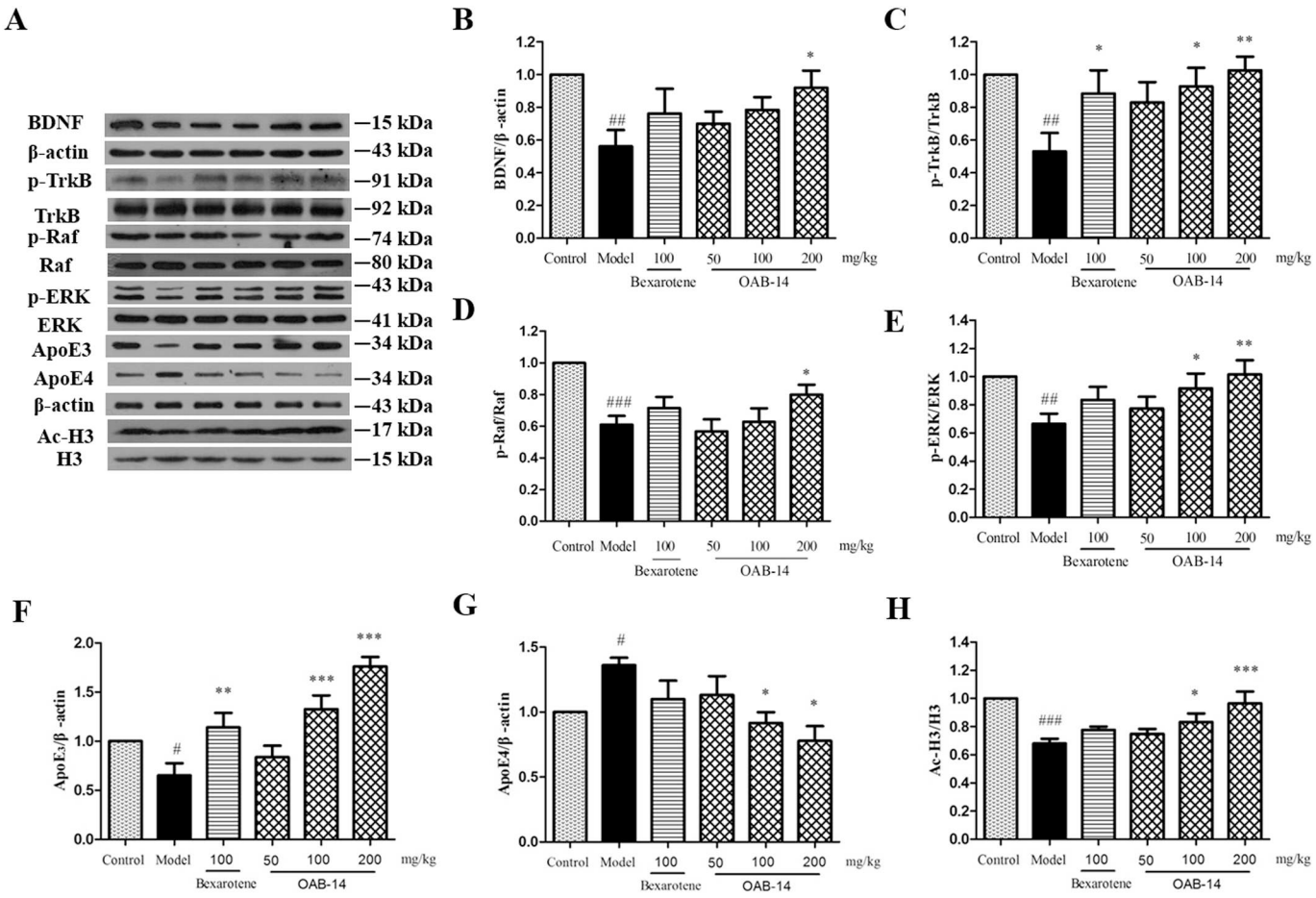

Fig. 16. OAB-14 activates the BDNF/TrkB/Raf/ERK pathway. (A) Representative Western blot. Quantification of (B) BDNF, (C) p-TrkB and total TrkB, (D) p-Raf and total Raf, (E) p-ERK1/2 and total ERK1/2, (F) ApoE3, (G) ApoE4, and (H) Ac-H3 and total H3 protein expression ($n = 5$). Data are presented as the mean ± SEM $^{\#}p < 0.05$, $^{\#\#}p < 0.01$ or $^{\#\#\#}p < 0.001$ vs. the control group and $^{*}p < 0.05$, $^{**}p < 0.01$ or $^{***}p < 0.001$ vs. the model group.

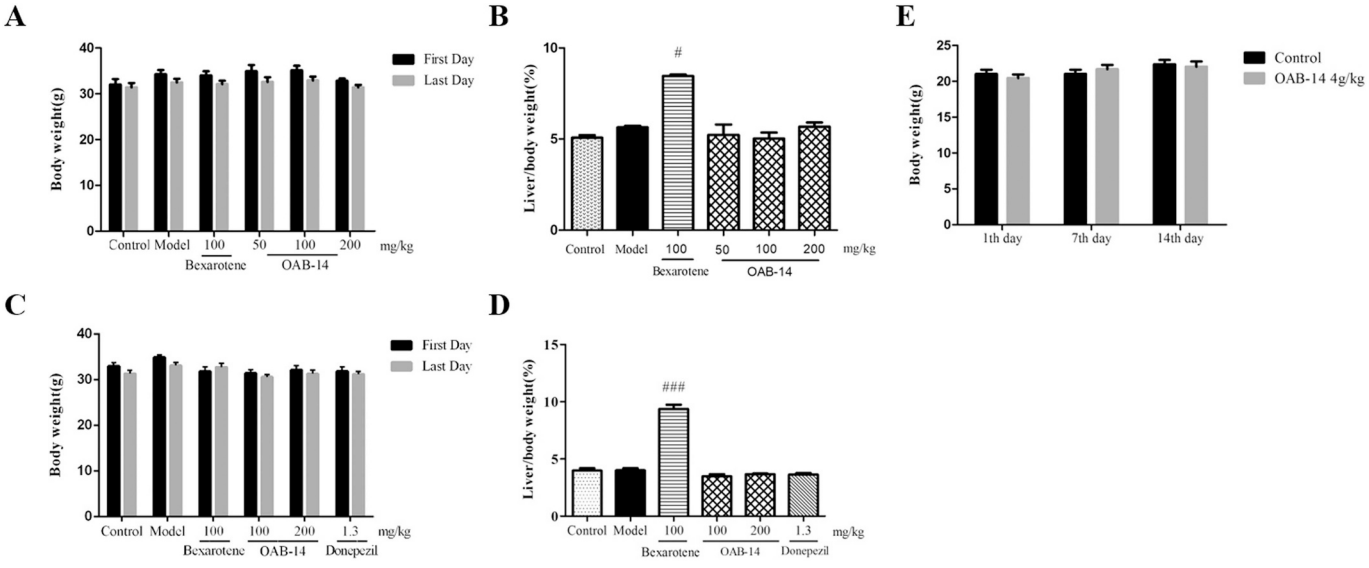

Fig. 17. OAB-14 does not change the body weight or liver index (liver/body weight) after acute and chronic treatment and does not change the body weight after the acute toxicity test. (A) Body weight ($n = 11$) and (B) liver index ($n = 5$) after acute treatment. (C) Body weight ($n = 11$) and (D) liver index ($n = 5$) after chronic treatment. (E) Body weight after acute toxicity test ($n = 20$). Data are presented as the mean ± SEM. $^{\#}p < 0.05$ or $^{\#\#\#}p < 0.001$ vs. the model group.

3.4. OAB-14 reduces the level of phosphorylated tau in the cerebral cortex of APP/PS1 mice

Overproduction of Aβ promotes tau hyperphosphorylation and the subsequent formation of NFTs. Since OAB-14 reduced Aβ levels in the brains of APP/PS1 mice, we asked whether tau hyperphosphorylation is affected by OAB-14 treatment. Higher levels of phosphorylated tau at Thr231, Ser396, and Ser404 were detected in APP/PS1 mice than in control mice (Thr231 $F_{5,24} = 5.505$, $p = 0.002$; post hoc test, $p = 0.000$; Ser 396 $F_{5,24} = 2.894$, $p = 0.035$; post hoc test, $p = 0.003$; Ser404 $F_{5,24} = 4.93$, $p = 0.003$; post hoc test, $p = 0.000$; Fig. 13B–D), whereas the levels of the total tau protein did not change. After acute treatment with OAB-14, the levels of phosphorylated tau were remarkably decreased in APP/PS1 mice (Thr231 $p = 0.001$; Ser 396 $p = 0.004$; Ser404 $p = 0.005$; Fig. 13B–D). We further examined the protein levels of glycogen synthase kinase-3β (GSK-3β), a primary kinase responsible for phosphorylating tau, and the PI3K/AKT pathway and the Wnt pathway, two upstream events that modulate GSK-3β activation. OAB-14 substantially increased the levels of p-PI3K, p-AKT and Wnt-3α compared with the model group (p-PI3K $F_{5,24} = 7.658$, $p = 0.000$; post hoc test, $p = 0.015$; p-AKT $F_{5,24} = 2.657$, $p = 0.048$; post hoc test, $p = 0.008$; Wnt-3α $F_{5,24} = 3.324$, $p = 0.02$; post hoc test, $p = 0.01$; Fig. 13F–H), whereas total PI3K and AKT levels were unchanged. These changes possibly resulted in the subsequent decrease in the levels of activated GSK-3β (Tyr216) (GSK-3β $F_{5,24} = 3.394$, $p = 0.018$; post hoc test, $p = 0.009$; Fig. 13E). Thus, we speculated that OAB-14 might inhibit GSK-3β activation (Tyr216) by increasing p-PI3K, p-AKT and Wnt-3α levels to subsequently reduce tau phosphorylation. Furthermore, acute treatment with OAB-14 remarkably decreased p-PP2A levels (Y307) ($F_{5,24} = 3.56$, $p = 0.015$; post hoc test, $p = 0.028$; Fig. 13I).

3.5. OAB-14 reverses neuronal loss in the hippocampus of APP/PS1 mice

$Aβ_{1–40}$ and $Aβ_{1–42}$ form soluble and insoluble Aβ aggregates that induce synaptic dysfunction and neuronal death, which are typically features observed in patients with AD. Hence, we asked whether OAB-14 exerted effects on neurons and synapses. We quantified the populations of neurons labelled with the NeuN marker to determine the effect of OAB-14 on CA1 neurons in the hippocampus of APP/PS1 mice. NeuN immunofluorescence staining revealed fewer neurons in APP/PS1 mice than in the control mice, and the decrease was rescued by acute treatment with OAB-14 to the level in the control mice ($F_{5,24} = 8.229$, $p = 0.000$; post hoc test, $p = 0.000$; Fig. 14A and B). The effect of OAB-14 on the neuron number was consistent with its effect on the levels of NeuN protein in Western blots ($F_{5,24} = 2.846$, $p = 0.037$; post hoc test, $p = 0.004$; Fig. 14C). In contrast, bexarotene only increased the number of neurons in the CA1 area of the hippocampus, but did not change the levels of NeuN protein in the cortex ($p = 0.381$; Fig. 14C), which is consistent with a previous report [24]. Furthermore, we also observed the ultrastructure of neuronal nuclei in the CA1 area of the hippocampus using transmission electron microscopy. The neuronal nuclei in the model group were damaged while OAB-14 repaired the damaged neuronal nuclei (Fig. 14D).

3.6. OAB-14 reverses synaptic degeneration and increases the expression of synapse-associated proteins

We used transmission electron microscopy to observe the ultrastructure of the synapses in the CA1 area of the hippocampus to further examine the effect of OAB-14 on synapses. The synaptic cleft became narrow, the number of synaptic vesicles in the presynaptic compartment was reduced in the model group compared with the control group, and most presynaptic and postsynaptic membranes were fused in the model group (Fig. 15A). However, OAB-14 partially reversed the degeneration of the synaptic architecture. The improvement in synaptic structure was accompanied by an increase in the levels of synapse-related proteins. Lower levels of synaptophysin (SYP), PSD95, and GAP43 were observed in the model group than in the control group, whereas the neurite outgrowth inhibitor A (Nogo A) did not significantly change (SYP $F_{5,24} = 2.825$, $p = 0.038$; post hoc test, $p = 0.002$; PSD95 $F_{5,24} = 2.676$, $p = 0.047$; post hoc test, $p = 0.012$; GAP43 $F_{5,24} = 5.706$, $p = 0.001$; post hoc test, $p = 0.000$; Nogo A $F_{5,24} = 1.749$, $p = 0.162$; Fig. 15C–F). After acute treatment with OAB-14, SYP, PSD95 and GAP43 levels were remarkably elevated compared with the model group, but Nogo A did not display obvious changes (SYP $p = 0.010$; PSD95 $p = 0.003$; GAP43 $p = 0.003$; Fig. 15C–F).

3.7. OAB-14 increases brain-derived neurotrophic factor (BDNF) expression and activates the BDNF signalling pathway in the cortex of APP/PS1 mice

Compared with the control mice, BDNF expression was prominently decreased in APP/PS1 mice ($F_{5,24} = 2.668$, $p = 0.047$; post hoc test, $p = 0.003$; Fig. 16B). The decrease of BDNF expression was rescued by OAB-14 acute treatment in APP/PS1 mice ($p = 0.014$, Fig. 16B). Furthermore, OAB-14 activated the BDNF/TrkB signalling pathway, followed by an increase in the levels of phosphorylated TrkB, Raf, ERK1/2, PI3K and AKT, without affecting total protein levels (p-TrkB/TrkB $F_{5,24} = 2.863$, $p = 0.036$; post hoc test, $p = 0.014$ for 100 mg/kg, $p = 0.003$ for 200 mg/kg; p-Raf/Raf $F_{5,24} = 6.187$, $p = 0.001$; post hoc test, $p = 0.049$; p-ERK/ERK $F_{5,24} = 2.679$, $p = 0.046$; post hoc test, $p = 0.043$ for 100 mg/kg, $p = 0.007$ for 200 mg/kg; Figs. 16C–E, 13F,G).

3.8. OAB-14 increases the levels of ApoE3 and acetylated histone 3 (H3) in the cortex of APP/PS1 mice

Protein levels of ApoE3 were decreased in APP/PS1 mice compared with control mice, whereas protein levels of ApoE4 were increased (ApoE3: $F_{5,24} = 11.527$, $p = 0.000$; post hoc test, $p = 0.043$; ApoE4: $F_{5,24} = 3.741$, $p = 0.012$; post hoc test, $p = 0.021$; Fig. 16F and G). Acute treatment with OAB-14 increased ApoE3 expression and reduced ApoE4 expression (ApoE3: $p = 0.000$; ApoE4: $p = 0.001$; Fig. 16F and G). We examined the levels of acetylated H3 using Western blotting. The ratio of acetylated H3 (Ac-H3) to H3 was dramatically decreased in the model group compared with the control group ($F_{5,24} = 7.062$, $p = 0.000$; post hoc test, $p = 0.000$; Fig. 16H). The acute OAB-14 treatment restored the level of acetylated H3 ($p = 0.000$; Fig. 16H).

3.9. Oral OAB-14 is safe

After three months of treatment with OAB-14, we did not observe abnormal behaviours and no animals died. Furthermore, we did not observe weight loss in APP/PS1 mice treated with bexarotene, a result that differs from a previous report [24]. However, the liver index (liver/body weight × 100%) was higher in the bexarotene-treated group than in the model group after acute ($F_{5,19} = 32.098$, $p = 0.000$; post hoc test, $p = 0.000$; Fig. 17B) and chronic treatment with OAB-14 ($F_{5,24} = 111.974$, $p = 0.000$; post hoc test, $p = 0.000$; Fig. 17D). Thus, bexarotene treatment induced hepatomegaly, which is likely due to hepatic failure. However, OAB-14 showed no evident effects on body weight or the liver index after acute (body weight: 1st day $F_{5,49} = 1.486$, $p = 0.212$; 15th day $F_{5,49} = 0.581$, $p = 0.715$; liver index: $p = 0.627$; Fig. 17A and B) and chronic treatment (body weight: 1st day $F_{5,60} = 2.244$, $p = 0.061$; 15th day $F_{5,60} = 2.034$, $p = 0.087$; liver index: $p = 0.285$; Fig. 17C and D). We conducted an acute toxicity test on C57 mice to further investigate the safety of OAB-14. Mice were continuously observed for 14 days after oral administration of 4.0 g/kg OAB-14. None of the animals died, and obvious toxic reactions and notable differences in body weight (Fig. 17E) were not observed in either the controls or the OAB-14 group. The maximum dose of drug

tolerated by mice was > 4.0 g/kg.

4. Discussion

Currently, the most accepted hypothesis regarding the aetiology of AD is the Aβ cascade hypothesis proposed by Hardy [25]. According to this hypothesis, large amounts of Aβ deposits appear in the brains of patients with AD as the disease progresses and are related to the memory disorders observed in patients with AD. APP/PS1 double transgenic mice, which mimic the pathological hallmarks of AD in terms of Aβ deposition, have been widely used as an animal model of AD. In this study, we investigated the therapeutic effects of OAB-14 on Aβ-related pathology in 8-month-old APP/PS1 mice. In the present study, we evaluated image discrimination memory using the NOR test and spatial learning and memory using the MWM test. Acute and chronic OAB-14 treatments exerted remarkable effects on cognitive impairments in APP/PS1 mice. Using Aβ antibody staining and thioflavin S staining, we observed that OAB-14 treatments significantly decreased Aβ deposits in the hippocampus and cortex; ELISA also revealed that OAB-14 treatments reduced the levels of soluble and insoluble Aβ in the cortex of APP/PS1 mice.

Since Aβ accumulation results from the imbalance between Aβ production and clearance, we first examined the effect of OAB-14 treatment on Aβ production. The levels of APP and enzymes responsible for generating Aβ, including ADAM10, BACE-1, and PS1, were not affected by acute OAB-14 treatment, but APP protein levels were reduced by chronic OAB-14 treatment, which might contribute to decreased Aβ accumulation. It is likely that the acute OAB-14 treatment did not exert significant effects on Aβ production, indicating a greater dependence on increased Aβ clearance.

The following three main mechanisms of Aβ clearance have been reported: enzyme-mediated Aβ degradation, including NEP, IDE, ECE, etc.; receptor-mediated Aβ transport; and microglia-dependent phagocytosis. Based on accumulating evidence, microglia internalize soluble and fibrillar Aβ in vivo and in vitro by phagocytosis [26]. Bexarotene increases the removal of soluble Aβ by microglia in an ApoE-dependent manner [10]. As the primary lipid transporter in the brain, ApoE possess three allelic isoforms, including ApoE2, ApoE3 and ApoE4 [27]. Among these isoforms, ApoE4 represents the strongest genetic risk factor for late-onset AD, increasing the risk of AD and reducing the age of AD onset [28], whereas ApoE3 improves synaptic plasticity and exerts a neuroprotective effect [29]. Although the role of ApoE in AD is not yet completely understood, ApoE has been reported to repair and regenerate the neuronal membrane [30], suppress the onset of Aβ deposition [31], and exert anti-inflammatory effects [32]. In particular, ApoE has recently been shown to carry a large number of lipids, and lipid-enriched ApoE promotes Aβ degradation and removal [32]. The ability of ApoE to remove Aβ depends on its isoforms and its lipidation status [33].

ABCA1 and ABCG1 are the most important ApoE-lipidating proteins, and ABCA1 mediates cholesterol transport to lipid-free apolipoproteins to produce nascent lipoproteins [34]. Partial lipidation of ApoE inhibits its interaction with ABCA1 [35]; therefore, ABCG1, but not ABCA1, further induces cholesterol efflux into nascent lipoproteins to form mature lipoproteins [36]. In fact, the absence of ABCA1 in transgenic mice increases the number of Aβ plaques by reducing the level of lipidated ApoE [30,37,38]. The esterification state of ApoE is key to its ability to clear Aβ. OAB-14 treatment increased ABCA1 and ApoE expression at 200 mg/kg, and ABCG1 expression at 100 and 200 mg/kg. However, interestingly, we were not able to repeat the results reported by Landreth and colleagues [10] that ABCA1 expression increased after 15 days of bexarotene treatment. Both OAB-14 and bexarotene treatments increased the levels of lipidated ApoE, which likely resulted from increased levels of ABCA1 and ABCG1. Lipidated ApoE and soluble Aβ combine to form the ApoE:Aβ complex, which was more susceptible to phagocytosis by microglia than ApoE-free Aβ [39]. Based on our results, the clearance of soluble Aβ by OAB-14 may be related to its ability to increase the levels of esterified ApoE. Additionally, we also found that OAB-14 increased NEP and IDE expression. The two enzymes also possibly contribute to the increased Aβ clearance induced by OAB-14 treatment. Interestingly, the capacity of IDE to degrade Aβ is also governed by the lipidation status of ApoE [33].

The causes of AD are complex, but several decades of research have shown that the development of AD is associated with neuronal inflammation, and the inflammatory response induced by Aβ is involved in AD development. OAB-14 promoted the transformation of proinflammatory M1 microglia into anti-inflammatory and phagocytosis-capable M2 microglia and increased Aβ clearance. Meanwhile, OAB-14 decreased the expression of inflammatory cytokines, thus suppressing two of the causes of AD.

The B class scavenger receptor CD36 acts as a fibrillar Aβ receptor [40]. In our studies, acute OAB-14 treatment caused a remarkable increase in CD36 expression on the surface of microglia, which might be the main reason why microglia remove fibrillar Aβ. CD36-positive microglia are M2 microglia [41], providing further validation for the hypothesis that OAB-14 promotes the conversion of microglia from the M1 to M2 phenotype.

As a microtubule-associated protein, the main function of the tau protein is to promote the polymerization of microtubules and to maintain their stability. However, hyperphosphorylated tau aggregates in cells to form NFTs, which are another hallmark of AD. Aβ has been shown to increase the phosphorylation of the tau protein. In the present study, OAB-14 increased Aβ clearance and decreased tau hyperphosphorylation at Thr231, Ser396 and Ser404, which might suppress the effects of Aβ toxicity on triggering tau hyperphosphorylation. Additionally, the mechanisms regulating the phosphorylation of tau protein are mainly divided into the following two categories: protein kinases that promote the phosphorylation of the tau protein (GSK-3β is the most important) and phosphatases involved in dephosphorylating the tau protein (includes PP2A, PP2B, PP1, and PP5, among others). Levels of p-GSK-3β (Tyr216, the phosphorylation of which increases GSK-3β activity) and p-PP2A (Y307, the phosphorylation of which inhibits PP2A activity) were remarkably decreased compared with those in the model group after acute treatment with OAB-14. Based on these results, OAB-14 potentially reduced tau hyperphosphorylation by possibly reducing Aβ deposition or by inhibiting the activation of GSK-3β and promoting the activation of PP2A.

Aβ overaccumulation in the AD brain may trigger neuronal loss and synaptic degeneration. APP/PS1 mice displayed a loss of synaptic proteins. OAB-14 increased the number of NeuN-positive cells and the levels of the NeuN protein, and attenuated the decrease in the levels of the synapse-related proteins SYP, GAP43, and PSD95 in APP/PS1 mice, suggesting that OAB-14 improves synaptic plasticity and ameliorates synapse and neuronal loss. Among the numerous neurotrophic factors, BDNF is the most widely distributed factor in the central nervous system. BDNF binds to its specific receptor TrkB, inducing the phosphorylation of the TrkB receptor. Activated receptors trigger the MEK/ERK and PI3K/AKT pathways, increasing the expression of synapse-related proteins [42,43]. Thus, we asked how OAB-14 affected the expression synapse-associated proteins. Notably, bexarotene was recently shown to exert neuroprotective effects and improve behaviours by activating the nuclear receptor Nurr1 and BDNF [44]. BDNF-TrkB signalling increased PSD95 expression [45]. In the present study, acute OAB-14 treatment indeed activated the BDNF/TrkB pathway, followed by the PI3K/AKT and Raf/MEK/ERK pathways to enhance synaptic plasticity. The strong neuroprotective effects of OAB-14 are likely mediated by its dual function in increasing the clearance of Aβ deposits and enhancing neurotrophin function.

ApoE3 was recently shown to increase the acetylation of histone H3 (Ac-H3) and then upregulate BDNF expression, whereas ApoE4 increases the expression of histone deacetylases, thereby reducing BDNF

expression. Furthermore, ApoE3 also blocks ApoE4-mediated down-regulation of BDNF [46]. Our results confirmed that OAB-14 increased ApoE3 expression, elevated the levels of acetylated H3, and subsequently increased BDNF expression. Additionally, OAB-14 also decreased ApoE4 expression and reduced its inhibitory effects on BDNF expression. ApoE3 activates the Aβ-degradation enzyme neprilysin [32]. ApoE3 not only inhibits GSK-3β activity by activating the PI3K/PKB pathway but also upregulates PSD95 and SYP to stimulate synaptogenesis. ApoE4 exerts the opposite effects. Moreover, ApoE interacts with its receptor LRP1 to exert an anti-inflammatory effect [47]. Thus, according to these reports, we propose the bold hypothesis that the ultimate mechanism by which OAB-14 improves cognitive impairments in APP/PS1 mice may be due to the increase of ApoE expression in the brain, particularly the expression of ApoE3. However, this hypothesis requires further validation in follow-up experiments.

5. Conclusion

In summary, OAB-14 significantly reduced Aβ accumulation and tau hyperphosphorylation, prevented neuronal loss and improved synaptic plasticity in APP/PS1 mice, potentially improving learning and memory deficits. Furthermore, we did not observe any abnormalities or toxicity in mice administered chronic and acute OAB-14 treatments. Therefore, OAB-14 represents a potential new candidate drug for the treatment of AD with further research value.

Conflicts of interest statement

The authors declare no competing financial interests.

Transparency document

The Transparency document associated with this article can be found, in online version.

Acknowledgements

This work was supported by grants from the National Science and Technology Major Special Project on Major New Drug Innovation of China (nos. 2009ZX09103-119 and 2009ZX09301-012). We thank the ELSEVIER Language Editing Services for its linguistic assistance during the preparation of this manuscript.

Author contributions

C.L.Y., X.L.G. and L.B.Z. designed the experiments. C.L.Y., X.L.G., X.Y.Z., H.L.L., J.X., S.M.Q. and Y.Y. conducted the experiments. Q.F.Z., F.Y.D., J.H.G., C.W.C. and G.L.C. synthesized OAB-14 and bexarotene. P.L., T.Y.C., X.F.J. and D.Y.L. analysed the data. G.L.C. and L.B.Z. helped conceive the project. C.L.Y. wrote the manuscript.

Appendix A. Supplementary data

Supplementary data to this article can be found online at https://doi.org/10.1016/j.bbadis.2018.10.028.

References

[1] M. Prince, A. Comas-Herrera, M. Knapp, M. Guerchet, M. Karagiannidou, World Alzheimer report 2016. Improving healthcare for people living with dementia: coverage, quality and costs now and in the future, https://www.alz.co.uk/research/world-report-2016.
[2] K. Blennow, M.J. de Leon, H. Zetterberg, Alzheimer's disease, Lancet 368 (2006) 387–403.
[3] J. Hardy, D.J. Selkoe, The amyloid hypothesis of Alzheimer's disease: progress and problems on the road to therapeutics, Science 297 (2002) 353–356.
[4] D.J. Selkoe, Normal and abnormal biology of the β-amyloid precursor protein, Annu. Rev. Neurosci. 17 (1994) 89–517.
[5] N.M. Hooper, A.J. Turner, The search for alpha-secretase and its potential as a therapeutic approach to Alzheimer's disease, Curr. Med. Chem. 9 (2002) 1107–1119.
[6] D.R. Riddell, G. Christie, I. Hussain, C. Dingwall, Compartmentalization of beta-secretase (Asp2) into low-buoyant density, noncaveolar lipid rafts, Curr. Biol. 1 (2001) 1288–1293.
[7] A. Mullard, BACE inhibitor bust in Alzheimer trial, Nat. Rev. Drug Discov. 16 (2017) 155.
[8] R.S. Doody, Rema Raman, Martin Farlow, Takeshi Iwatsubo, Bruno Vellas, Steven Joffe, et al., A phase 3 trial of semagacestat for treatment of Alzheimer's disease, N. Engl. J. Med. 369 (2013) 341.
[9] L.S. Honig, B. Vellas, M. Woodward, M. Boada, R. Bullock, M. Borrie, et al., Trial of solanezumab for mild dementia due to Alzheimer's disease, N. Engl. J. Med. 378 (2018) 321–330.
[10] P.E. Cramer, J.R. Cirrito, D.W. Wesson, C.Y. Lee, J.C. Karlo, A.E. Zinn, et al., ApoE-directed therapeutics rapidly clear β amyloid and reverse deficits, Science 335 (2012) 1503–1506.
[11] N.F. Fitz, A.A. Cronican, I. Lefterov, R. Koldamova, Comment on "ApoE-directed therapeutics rapidly clear beta-amyloid and reverse deficits in AD mouse models", Science 340 (2013) 924-c.
[12] A.R. Price, G. Xu, Z.B. Siemienski, L.A. Smithson, D.R. Borchelt, T.E. Golde, et al., Comment on "ApoE-directed therapeutics rapidly clear beta-amyloid and reverse deficits in AD mouse models", Science 340 (2013) 924-d.
[13] I. Tesseur, A.C. Lo, A. Roberfroid, S. Dietvorst, B. Van Broeck, M. Borgers, et al., Comment on "ApoE-directed therapeutics rapidly clear beta-amyloid and reverse deficits in AD mouse models", Science 340 (2013) 924-e.
[14] K. Veeraraghavalu, C. Zhang, S. Miller, J.K. Hefendehl, T.W. Rajapaksha, J. Ulrich, et al., Comment on "ApoE-directed therapeutics rapidly clear beta-amyloid and reverse deficits in AD mouse models", Science 340 (2013) 924-f.
[15] L. Mucke, D.J. Selkoe, Neurotoxicity of amyloid β-protein: synaptic and network dysfunction, Cold Spring Harb. Perspect. Med. 2 (2012) a006338.
[16] D.M. Walsh, D.J. Selkoe, Deciphering the molecular basis of memory failure in Alzheimer's disease, Neuron 44 (2004) 181–193.
[17] M. Ahmed, J.B.T. Rocha, M. Corrêa, C.M. Mazzanti, R.F. Zanin, A.L.B. Morsch, et al., Inhibition of two different cholinesterases by tacrine, Chem. Biol. Interact. 162 (2006) 165–171.
[18] J.H. Barnard, J.C. Collings, A. Whiting, S.A. Przyborski, T.B. Marder, Synthetic retinoids: structure-activity relationships, Chemistry 15 (2010) 11430–11442.
[19] K.M. Frick, J.E. Gresack, Sex differences in the behavioral response to spatial and object novelty in adult C57BL/6 mice, Behav. Neurosci. 117 (2003) 1283–1291.
[20] G. Jin, L.H. Wang, X.F. Ji, T.Y. Chi, Y. Qi, Q. Jiao, et al., Xanthoceraside rescues learning and memory deficits through attenuating beta-amyloid deposition and tau hyperphosphorylation in APP mice, Neurosci. Lett. 573 (2014) 58–63.
[21] X.F. Ji, T.Y. Chi, Q. Xu, X.L. He, X.Y. Zhou, R. Zhang, et al., Xanthoceraside ameliorates mitochondrial dysfunction contributing to the improvement of learning and memory impairment in mice with intracerebroventricular injection of $A\beta_{1-42}$, Evid. Based Complement. Alternat. Med. 2014 (2014) 969342.
[22] M. Filali, R. Lalonde, S. Rivest, Subchronic memantine administration on spatial learning, exploratory activity, and nest-building in an APP/PS1 mouse model of Alzheimer's disease, Neuropharmacology 60 (2011) 930–936.
[23] A.W. Corona, N. Kodoma, B.T. Casali, G.E. Landreth, ABCA1 is necessary for bexarotene-mediated clearance of soluble amyloid beta from the hippocampus of APP/PS1 mice, J. NeuroImmune Pharmacol. 11 (2016) 61–72.
[24] M. Tachibana, M. Shinohara, Y. Yamazaki, C.C. Liu, J. Rogers, G. Bu, et al., Rescuing effects of RXR agonist bexarotene on aging-related synapse loss depend on neuronal LRP1, Exp. Neurol. 277 (2015) 1–9.
[25] J.A. Hardy, G.A. Higgins, Alzheimer's disease: the amyloid cascade hypothesis, Science 256 (1992) 184–185.
[26] J. Rogers, R. Strohmeyer, C.J. Kovelowski, R. Li, Microglia and inflammatory mechanisms in the clearance of amyloid beta peptide, Glia 40 (2002) 260–269.
[27] M.P. Burns, L. Vardanian, A. Pajoohesh-Ganji, L. Wang, M. Cooper, D.C. Harris, et al., The effects of ABCA1 on cholesterol efflux and Aβ levels in vitro and in vivo, J. Neurochem. 98 (2006) 792–800.
[28] C.C. Liu, T. Kanekiyo, H. Xu, G. Bu, Apolipoprotein E and Alzheimer disease: risk, mechanisms and therapy, Nat. Rev. Neurol. 9 (2013) 106–118.
[29] J. Kim, H. Yoon, J. Basak, J. Kim, Apolipoprotein E in synaptic plasticity and Alzheimer's disease: potential cellular and molecular mechanisms, Mol. Cell 37 (2014) 767–776.
[30] S.E. Wahrle, H. Jiang, M. Parsadanian, R.E. Hartman, K.R. Bales, S.M. Paul, et al., Deletion of Abca1 increases Aβ deposition in the PDAPP transgenic mouse model of Alzheimer disease, J. Biol. Chem. 280 (2005) 43236–43242.
[31] M. Morikawa, J.D. Fryer, P.M. Sullivan, E.A. Christopher, S.E. Wahrle, R.B. DeMattos, et al., Production and characterization of astrocyte-derived human apolipoprotein E isoforms from immortalized astrocytes and their interactions with amyloid-β, Neurobiol. Dis. 19 (2005) 66–76.
[32] M. Bodzioch, E. Orsó, J. Klucken, T. Langmann, A. Böttcher, W. Diederich, et al., The gene encoding ATP-binding cassette transporter 1 is mutated in Tangier disease, Nat. Genet. 22 (1999) 347–351.
[33] Q. Jiang, C.Y. Lee, S. Mandrekar, B. Wilkinson, P. Cramer, N. Zelcer, et al., ApoE promotes the proteolytic degradation of Aβ, Neuron 58 (2008) 681–693.
[34] S.E. Wahrle, H. Jiang, M. Parsadanian, J. Legleiter, X. Han, J.D. Fryer, et al., ABCA1 is required for normal central nervous system ApoE levels and for lipidation of astrocyte-secreted apoE, J. Biol. Chem. 279 (2004) 40987–40993.
[35] L. Krimbou, M. Denis, B. Haidar, M. Carrier, M. Marcil, J. Genest Jr., Molecular interactions between ApoE and ABCA1: impact on ApoE lipidation, J. Lipid Res. 45 (2004) 839–848.

[36] B. Karten, R.B. Campenot, D.E. Vance, J.E. Vance, Expression of ABCG1, but not ABCA1, correlates with cholesterol release by cerebellar astroglia, J. Biol. Chem. 281 (2006) 4049–4057.
[37] V. Hirsch-Reinshagen, L.F. Maia, B.L. Burgess, J.F. Blain, K.E. Naus, S.A. Mclsaac, et al., The absence of ABCA1 decreases soluble ApoE levels but does not diminish amyloid deposition in two murine models of Alzheimer disease, J. Biol. Chem. 280 (2005) 43243–43256.
[38] R. Koldamova, M. Staufenbiel, I. Lefterov, Lack of ABCA1 considerably decreases brain ApoE level and increases amyloid deposition in APP23 mice, J. Biol. Chem. 280 (2005) 43224–43235.
[39] C. Russo, G. Angelini, D. Dapino, A. Piccini, G. Piombo, G. Schettini, et al., Opposite roles of apolipoprotein E in normal brains and in Alzheimer's disease, Proc. Natl. Acad. Sci. U. S. A. 95 (1998) 15598–15602.
[40] I.S. Coraci, J. Husemann, J.W. Berman, C. Hulette, J.H. Dufour, G.K. Campanella, et al., CD36, a class B scavenger receptor, is expressed on microglia in Alzheimer's disease brains and can mediate production of reactive oxygen species in response to beta amyloid fibrils, Am. J. Pathol. 160 (2002) 101–112.
[41] K. Kawahara, M. Suenobu, A. Yoshida, K. Koga, A. Hyodo, H. Ohtsuka, et al., Intracerebral microinjection of interleukin-4/interleukin-13 reduces β-amyloid accumulation in the ipsilateral side and improves cognitive deficits in young amyloid precursor protein 23 mice, Neuroscience 207 (2012) 243–260.
[42] W. Li, J. Keifer, Rapid enrichment of presynaptic protein in boutons undergoing classical conditioning is mediated by brain-derived neurotrophic factor, Neuroscience 203 (2012) 50–58.
[43] C. Robinet, L. Pellerin, Brain-derived neurotrophic factor enhances the hippocampal expression of key postsynaptic proteins in vivo including the monocarboxylate transporter MCT2, Neuroscience 192 (2011) 155–163.
[44] K. Ghosal, M. Haag, P.B. Verghese, T. West, T. Veenstra, J.B. Braunstein, et al., A randomized controlled study to evaluate the effect of bexarotene on amyloid-β and apolipoprotein E metabolism in healthy subjects, Alzheimers Dement. 2 (2016) 110–120.
[45] A. Yoshii, M. Constantine-Paton, Postsynaptic localization of PSD-95 is regulated by all three pathways downstream of TrkB signaling, Front Synaptic Neurosci. 6 (2014) 1–7.
[46] A. Sen, T.J. Nelson, D.L. Alkon, ApoE4 and Aβ oligomers reduce BDNF expression via HDAC nuclear translocation, J. Neurosci. 35 (2015) 7538–7551.
[47] A. Pocivavsek, M.P. Burns, G.W. Rebeck, Low-density lipoprotein receptors regulate microglial inflammation through c-Jun N-terminal kinase, Glia 57 (2009) 444–453.